Stockholm University

NMR spectroscopy and MD simulations of carbohydrates

Elin Säwén

Cover picture: Five repeating units of the exopolysaccharide produced by *Streptococcus thermophilus* ST1 and a ^{1}H NMR spectrum of the same exopolysaccharide.

ISSN XXXX-XXXX
ISBN XXX-XX-XXXXX-XX-X

Printed in Sweden by US-AB, Stockholm 2011
Distributor: Department of Organic Chemistry, Stockholm University

Till *Ingrid*

Abstract

Knowledge about the structure, conformation and dynamics of carbohydrates is important in our understanding of the way carbohydrates function in biological systems, for example in intermolecular signaling and recognition. This thesis is a summary of five papers studying these properties in carbohydrate-containing molecules with NMR spectroscopy and molecular dynamics simulations.

In paper I, the ring-conformations of the six-membered rings of two carbaiduronic analogs were investigated. These carbasugars could potentially be used as hydrolytically stable mimics of iduronic acid in drugs. The study showed that the equilibrium is entirely shifted towards the $^4C_1$ conformation.

Paper II is an investigation of the conformational flexibility and dynamics of two (1→6)-linked disaccharides related to an oligosaccharide epitope expressed on malignant tumor cells.

In paper III, the conformational space of the glycosidic linkage of the disaccharide α-D-Man*p*-(1→2)-α-D-Man*p*-OMe, which is present in *N*- and *O*-linked glycoproteins, was studied. A maximum entropy analysis using different priors as background information was used and four new Karplus equations for $^3J_{C,C}$ and $^3J_{C,H}$ coupling constants, related to the glycosidic linkage, were presented.

Paper IV describes a structural elucidation of the exopolysaccharide (EPS) produced by *Streptococcus thermophilus* ST1, a major dairy starter used in yoghurt and cheese production. The EPS contains a hexasaccharide repeating unit of D-galactose and D-glucose residues, which is a new EPS structure of the *S. thermophilus* species.

In paper V, the dynamics of three generations of glycodendrimers were investigated by NMR diffusion and ^{13}C NMR relaxation studies. Three different correlations times were identified, one global correlation time describing the rotation of the dendrimer as a whole, one local correlation time describing the reorientation of the C-H vectors, and one correlation time describing the pulsation of a dendrimer branch.

List of publications

This thesis is based on the following papers, which are referred to in the text by their roman numerals.

I **Synthesis and conformational analysis of carbasugar bioisosteres of α-L-iduronic acid and its methyl glycoside**
Elin Säwén, Mattias U. Roslund, Ian Cumpstey, and Göran Widmalm
Carbohydrate Research, **2010**, 345, 984 – 993

II **Conformational flexibility and dynamics of two (1→6)-linked disaccharides related to an oligosaccharide epitope expressed on malignant tumour cells**
Ulrika Olsson, Elin Säwén, Roland Stenutz, and Göran Widmalm
Chemistry—A European Journal, **2009**, 15, 8886 – 8894

III **Population distribution of flexible molecules from maximum entropy analysis using different priors as background information: application to the *φ,ψ*–conformational space of the α-(1→2)-linked mannose disaccharide present in *N*- and *O*-linked glycoproteins**
Elin Säwén, Tariq Massad, Clas Landersjö, Peter Damberg, and Göran Widmalm
Organic and Biomolecular Chemistry, **2010**, 8, 3684 – 3695

IV **Structural analysis of the exopolysaccharide produced by *Streptococcus thermophilus* ST1 solely by NMR spectroscopy**
Elin Säwén, Eine Huttunen, Xue Zhang, Zhennai Yang, and Göran Widmalm
Journal of Biomolecular NMR, **2010**, 47, 125 – 134

V **The dynamics of GATG glycodendrimers by NMR diffusion and quantitative ^{13}C relaxation**
Ramon Novoa-Carballal, Elin Säwén, Eduardo Fernandez-Megia, Juan Correa, Ricardo Riguera, and Göran Widmalm
*Physical Chemistry Chemical Phys*ics, **2010**, 12, 6587 – 6589

Reprints of the papers were made with permission from the publishers.

Papers not included in this thesis:

Molecular conformations in the pentasaccharide LNF-1 derived from NMR spectroscopy and molecular dynamics simulations
Elin Säwén, Baltzar Stevensson, Jennie Östervall, Arnold Maliniak, and Göran Widmalm
Journal of Physical Chemistry B. **2011***,* 115, 7109–7121

Conformational properties of methyl β-maltoside and methyl α- and β-cellobioside disaccharides
Elizabeth Hatcher, Elin Säwén, Göran Widmalm, and Alexander D. MacKerell, Jr.
Journal of Physical Chemistry B. **2011,** 115, 597–608

Complete ^{1}H and ^{13}C NMR chemical shift assignments of mono-, di-, and trisaccharides as basis for NMR chemical shift predictions of polysaccharides using the computer program CASPER
Mattias U. Roslund, Elin Säwén, Jens Landström, Jerk Rönnols, K. Hanna M. Jonsson, Magnus Lundborg, Mona V. Svensson, and Göran Widmalm
Carbohydrate Research, **2011,** 346, 1311–1319

Synthesis of aromatic C-xylosides by position inversion of glucose
Jesper Malmberg, Katrin Mani, Elin Säwén, Anders Wirén, and Ulf Ellervik
Bioorganic and Medicinal Chemistry, **2006,** 14, 6659–6665

Contents

1 Introduction

1.1 General introduction to carbohydrates

Carbohydrates are the most abundant class of biomolecules in nature, functioning as energy storage (starch, glycogen), structural components of plants (cellulose), and being the major constituent of shells, insects, crabs, *etc.* (chitin). In the form of glycoconjugates, *i.e.*, carbohydrates covalently linked to other chemical species, carbohydrates are involved in far more advanced systems. The surface of cells is to a great extent covered with carbohydrates where they operate in cell–cell recognition and as storage of biological information.[1]

In contrast to other important biomolecules such as proteins and nucleic acids carbohydrates can form branched structures, by substitution of one or several hydroxyl groups, making them extremely complex and heterogeneous. The structure of an oligosaccharide is determined by the monosaccharide sequence, the glycosidic linkage sites and the stereochemistry of the glycosidic linkage (α or β).[1] The diversity of carbohydrate structures that occur in nature is further increased by derivatization of the ring hydroxyl groups, such as *O*-methylation and *O*-sulfation.

1.2 Glycoconjugates

In nature, glycoconjugates are ubiquitously found as part of proteins, bacteria and viruses. The extent to which a glycoconjugate is glycosylated can vary largely, with a carbohydrate content of 1% to 99%. The major classes of glycoconjugates found in nature are glycoproteins, proteoglycans, glycolipids and lipopolysaccharides.

1.2.1 Glycoproteins

A glycoprotein is a protein which has one or several oligosaccharides covalently linked to it. In animals, only a small number (~10) of monosaccharide variants contribute to the biosynthesis of glycoproteins. The variety of the oligosaccharides is still great. Glycoproteins are classified according to the linkage type of the oligosaccharide to the protein. The linkage can be to ei-

ther an asparagine residue, called *N*-linked glycoproteins or to a serine or a threonine residue, called *O*-linked glycoproteins, see *Figure 1.1*.

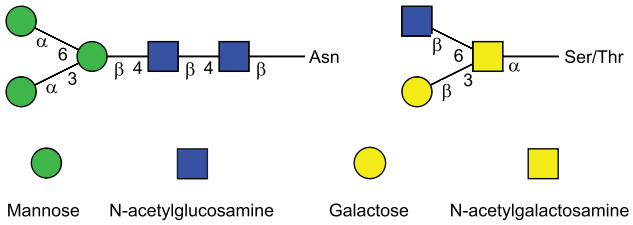

Figure 1.1. Schematic picture in CFG notation of the uniform core pentasaccharide of *N*-glycans (left), consisting of two GlcNAc and three mannose moieties. To the right is an example of an *O*-glycan belonging to the core II class, a GalNAc residue is bound to the peptide chain.

When attached to the cell membrane via an ethanolamine phosphate group they are called GPI anchors. The properties of a protein change with different glycosylation patterns. Often glycoproteins are embedded in the outer membrane of cells and work as antennas sticking out of the surface. They play a variety of roles in processes such as cell adhesion and the three-dimensional folding of proteins.[1, 2]

1.2.2 Proteoglycans

Proteoglycans are a class of proteins situated on the surface of cells. They make up a major part of the extracellular matrix, which provides structural support. Proteoglycans are also involved in binding cations and water, and in regulating the movement of molecules through the matrix. Proteoglycans are glycoproteins consisting polysaccharides covalently attached along the length of a single core protein. At least one of the polysaccharide chains of a proteoglycan must be a glycosaminoglycan (GAG). Proteoglycans vary greatly in size depending on the core protein's molecular weight and the number and length of the polysaccharide chains and can contain as much as 95% carbohydrates.

Glycosaminoglycans (GAG) are long unbranched polysaccharide chains consisting of repeating disaccharide units. By definition, one of the two sugars in the repeating disaccharide unit is an amino sugar, giving glycosaminoglycans their name. The other monosaccharide in the repeating unit is a uronic acid (glucuronic acid or iduronic acid) or a galactose. GAGs are divided into different classes due to the nature of their repeating unit; hyaluronan (HA), keratan sulfate (KS), chondrotin sulfate (CS), heparan sulfate (HS), heparin and dermatan sulfate (DA).[2]

1.2.3 Bacterial polysaccharides

Polysaccharides make up a substantial part of bacterial cell-walls, the greatest part being peptidoglycans giving the membrane mechanical strength. Other polysaccharides, such as lipopolysaccharides, capsular polysaccharides and exopolysaccharides, are to a large extent covering the cell-walls of bacteria. Microbial surface polysaccharides play an important role in bacteria-host interactions.

In gram-negative bacteria the lipid bilayer contains lipopolysaccharides (LPS's). LPS's consist of three regions, the lipid-A, the core region and the O-antigen. When the lipid-A is released from the membrane it is toxic and harmful to mammals. The O-antigen consists of repeating units with 2-8 carbohydrate moieties, and is very diverse. The O-antigen is the part of the bacteria recognized by the immune system.[1]

Bacteria can also produce capsular polysaccharides, which is an extracellular coat surrounding the bacteria associated with virulence.[2] An additional kind of polysaccharide produced by bacteria is exopolysaccharides (EPS). They are high molecular weight polymers generally composed of repeating units of D-glucose, D-mannose, D-galactose, L-fucose, L-rhamnose, and D-glucuronic acid.[3] Exopolysaccharides are used in a number of industrial products, *e.g.*, as food additives and in medical applications.[4]

1.2.4 Synthetic carbohydrates

Synthetic carbohydrates are used in many different ways. For instance; to evaluate their three-dimensional structure, for testing of biological activity and to map carbohydrate binding sites in proteins.[1] They are also crucial in the development of new carbohydrate-based drugs and vaccines as well as drug delivery systems. To enable and facilitate analysis with NMR spectroscopy it is sometimes necessary to synthesize isotopically labeled carbohydrates.

Oligosaccharides are traditionally synthesized in solution from the linking of a glycosyl donor with a glycosyl acceptor, an example is shown in *Figure 1.2*. The preparation of monosaccharide building blocks often involves tedious protecting group chemistry. More recently chemoenzymatic methods and automated solid-phase synthesis have facilitated the synthesis of oligosaccharides.[5]

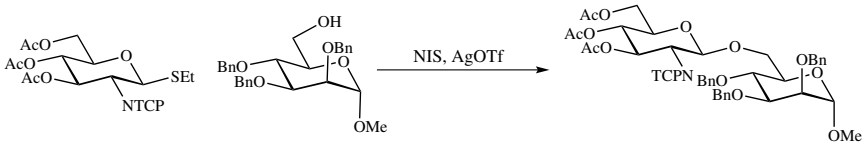

Figure 1.2. An example of a classical glycosylation reaction yielding β-D-Glc*p*NAc-(1→6)-α-D-Man*p*-OMe.

To make carbohydrates more useful as drugs they can be prepared as pseudo sugars where either the ring oxygen is replaced with a methylene group or the glycosidic oxygen is replaced by nitrogen, carbon or sulfur making them hydrolytically stable.[6]

Glycodendrimers are another example of carbohydrate-containing molecules. They are branched symmetrical polymers, often synthesized with click-chemistry.[7] Dendrimers have found many different uses, such as: host-guest chemistry, in catalysis, in materials science and as drug delivery systems.[8]

1.3 Monosaccharide structure

Carbohydrate is the general name of "hydrated carbons", compounds that often have the empirical formula $C_n(H_2O)_n$. A monosaccharide is an aldehyde or a ketone containing at least two additional hydroxyl groups. Two monosaccharides connected by a glycosidic bond are named a disaccharide; carbohydrates with three to ten units are typically called oligosaccharides while larger structures are known as polysaccharides. Carbohydrates are chiral and optically active; if a monosaccharide has the same absolute configuration at the highest numbered chiral carbon as D-glyceraldehyde, that compound is labeled D; those with opposite configuration are labeled L. The majority of natural occurring carbohydrates have the D-configuration.[9]

Carbohydrates with five or six carbon atoms, pentoses and hexoses, can form intramolecular hemiacetals between the carbonyl group and the hydroxyl group on carbon 4 or 5. The rings formed are called pyranoses (six-membered rings) or furanoses (five-membered rings). The cyclic and the acyclic forms exist in equilibrium where the hemiacetals are the most abundant forms. Upon hemiacetal formation, the former carbonyl carbon becomes a new stereocenter, called the anomeric center, with the hydroxyl group either equatorial (β in D-glucose) or axial (α in D-glucose). The equilibrium between the cyclic and acyclic forms allows the two anomeric forms to interconvert, a process called mutarotation.[10]

For pyranoses, as for cyclohexane, the six-membered ring can exhibit different conformations. For the majority of carbohydrates, the most energetically favored ring conformation is the chair conformation, which exists in two distinct forms, the $^4C_1$ and the $^1C_4$, where the *C* stands for chair and the numbers refers to the atoms above and below a reference plane. The $^4C_1$ conformation is generally favored for D-sugars due to fewer non-bonding interactions between the ring substituents. The six-membered ring can also exist in boat (*B*), half chair (*H*) and skew (*S*) conformations. Four possible ring conformations are shown in *Figure 1.3*. For D-Glc*p*, the $^4C_1$ conformation is the only one observed by NMR spectroscopy.[11] In some cases more ring conformations are present, for iduronic acid, for example, three low-energy conformations are in equilibrium, $^1C_4$, ^2S_O and $^4C_1$.[12]

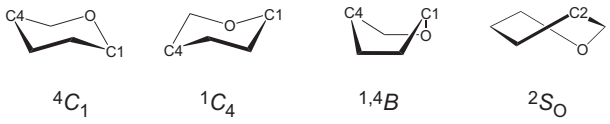

Figure 1.3. The two chair conformations, a boat conformation and a skew-boat conformation.

Glucopyranose exists in a 36:64 mixture between α and β forms in aqueous solutions; more electronegative substituents prefer the axial position. From steric reasons alone, the opposite would be expected. This higher than expected occurrence of the axial form is due to the anomeric effect. The most widely accepted explanation of the anomeric effect is that hyperconjugation stabilizes the axial conformation.[9] The lone pair electrons in the non-bonding endocyclic oxygen orbital (the n–orbital) donates electrons to the anti-bonding orbital (σ*) on the anomeric carbon, shortening the C1-O5 bond and lengthening the C1-O1 bond.[13]

1.4 Oligosaccharide conformation

Disaccharides and larger oligo- or polysaccharides have two or three extra degrees of freedom compared to monosaccharides, due to the orientation of the glycosidic linkage, which is described by the three torsion angles, phi (ϕ), psi (ψ) and omega (ω) (*Figure 1.4*).

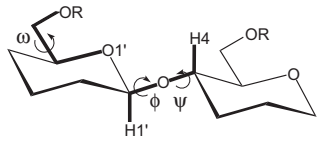

Figure 1.4. The three main degrees of freedom in an oligosaccharide, ϕ, ψ and ω.

The torsion angle definitions used in this thesis are in accordance with the NMR spectroscopy definition and in contrast to the IUPAC definition that uses heavy atoms.[9] ϕ is defined as the torsion angle H1–C1–O–$C_{aglycon}$, and is influenced by the *exo*-anomeric effect (see below) as well as by sterics effects. ψ is the rotation around O–$C_{aglycon}$ bond and is defined as C1–O–$C_{aglycon}$–$H_{aglycon.}$ It is influenced by steric effects and is typically around −50° or +50°. The ω–torsion angle defines 1→6 linked oligosaccharides and is the most flexible of the three. This torsion angle is defined by O5–C5–C6–O6 and is affected by steric interactions between hydroxyl groups in position 4 and 6 and by the gauche effect (*Figure 1.6*).[10]

The *exo*-anomeric effect mentioned above is an electronic effect between the exocyclic oxygen and C1. It originates from the same kind of favorable orbital overlap as the anomeric effect, the lone pair orbital on the $O_{aglycon}$

interacts with the σ* anti-bonding orbital between C1-O5. Two conformations are stabilized by this effect in the α and β forms respectively, with a preference for the syn conformation, *i.e.* ϕ = +60º for β-D-glycosides and ϕ = –60º α-D-glycosides, although the anti-conformation is sometimes also found.[14] In *Figure 1.5*, two of the stabilized conformations are shown.[9]

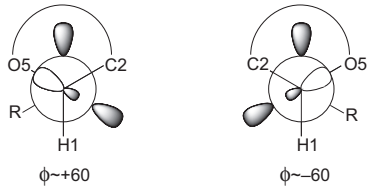

Figure 1.5. Schematic picture of two of the conformations stabilized by the *exo*-anomeric effect. The lone pair orbital on $O_{aglycon}$ is interacting with the anti-bonding orbital on C1. To the left is the β-form and to the right is the α-form.

For the ω–torsion angle around the C5–C6 bond, three different conformers can be considered, see *Figure 1.6*. The electronegative groups are in two cases gauche to each other, *i.e.*, separated by ~60º. The CH_2 group is prochiral, the two hydrogens named pro-*R* and pro-*S*. The three rotamers are labeled *gt* (gauche-trans), *gg* (gauche-gauche) and *tg* (trans-gauche). The *gt* and *gg* rotamers are dominant and their stability can be explained by hyperconjugation where the C–H σ-bonding orbital donates electrons to the C-O σ* anti-bonding orbital, thus having a stabilizing effect.[15]

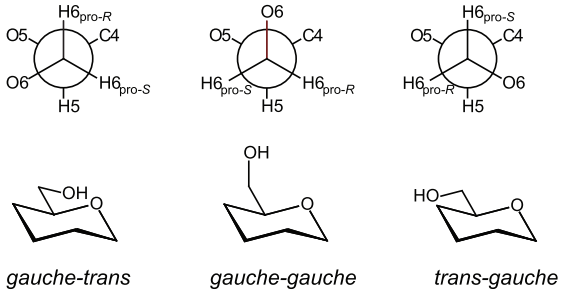

Figure 1.6. The three staggered rotamers. In *gt* rotamer ω = +60°. In glucose this is the major rotamer populated to 54%. The *gg* rotamer, ω = −60°, is populated to 45%. In the *tg* rotamer O5 and O6 are trans to each other, an unfavorable interaction which explains the low population of this rotamer.

1.5 Studies of conformation and dynamics

Knowledge about conformation and dynamics of carbohydrates is important in the understanding of interactions between molecules, for example, carbohydrates and proteins. In nature, these interactions take place in water. It is

for that reason important to study oligosaccharide conformation in water, which is possible with NMR spectroscopy. Another technique used to obtain information about the conformation of molecules is crystallography where a solid state structure is analysed, which does not give information about the flexibility of molecules. On the other hand, large collections of related structures with common fragments can give population distributions similar to those observed in solution.[16] Oligosaccharides are dynamic, flexible molecules in aqueous solution. In particular, the glycosidic linkage is rather flexible and is often described by several conformations. The transition between different conformations is in the order of nanoseconds and thus an average of the conformations present is seen in NMR spectroscopy. To gain more information about the distribution between the different conformations, molecular dynamic (MD) simulations and NMR spectroscopy are often used as complement to each other.

2 Nuclear magnetic resonance spectroscopy

2.1 Introduction

Nuclear magnetic resonance (NMR) spectroscopy is a very powerful tool in chemistry. It is routinely used for structural elucidation and characterization of synthetic products and natural compounds. NMR spectroscopy is also very useful in stereochemical and conformational investigations and in the study of dynamic systems. One big advantage of this technique is that it is non-destructive and all of the material used in the analysis can be recovered. The experiments can also be carried out in different solvents, including water, making it possible to mimic nature.[9]

NMR spectroscopy is based on the fact that nuclei possess an intrinsic property called spin. When a molecule is placed in a strong magnetic field a small fraction of all the spins align with the field resulting in a slight net alignment parallel to the field. In the magnetic field the energy of the spin states will differ. When these energy levels are perturbed a signal becomes detectable and gives rise to information about individual atoms in a molecule and their environment.[17]

2.2 Structure elucidation

When determining the structure of polysaccharides, the identities and the absolute configuration of the monosaccharide units are often the first to be investigated. The classical way to determine the components of a polysaccharide is to hydrolyze it to its reducing monosaccharides and convert these to alditol acetates, which are subsequently analyzed by gas chromatography. When the absolute configuration is determined, the reducing sugars are converted to chiral butyl glycosides prior to acetylation. However, the identification of monosaccharide units can also be performed by NMR spectroscopy by analyzing the chemical shifts and the coupling patterns of the different spin systems. Also, the monosaccharide components, their absolute configuration and the relative proportions can be determined by ^{1}H NMR spectroscopy using chiral derivatives of the constituent monosaccharides.[18]

A starting point when elucidating the structure of a polysaccharide by NMR spectroscopy is the proton and carbon chemical shifts obtained from

1D ^{1}H and ^{13}C NMR spectra or a 2D ^{1}H,^{13}C HSQC NMR spectrum. An alternative to the conventional Fourier transformed HSQC experiment is a Hadamard transformed (HT) HSQC experiment[19], see *Figure 2.1*. The evolution time is replaced by a number of selective carbon pulses encoded as on or off according to a Hadamard matrix. This type of experiment is several times faster than a regular HSQC experiment and gives higher resolution in the ^{13}C dimension.

From the anomeric resonances (4.4–5.5 ppm for proton and 90–110 ppm for carbon), information about the number of monosaccharide components in the repeating unit of the polysaccharide can be obtained. To investigate the signals of the ring resonances, 2D techniques such as ^{1}H,^{1}H TOCSY or ^{1}H,^{1}H COSY experiments, as well as selective 1D ^{1}H,^{1}H TOCSY experiments can be used. With these experiments, each spin system can be investigated individually and the ring resonances can be assigned. A H2BC experiment can also be very useful when elucidating a structure. It shows heteronuclear two-bond correlations and is complementary to TOCSY and HMBC experiments. When faced with severe overlap, it can be helpful to record a 2D HSQC-TOCSY spectrum to get additional dispersion though the carbon dimension. To further increase the dispersion, without the use of 3D spectroscopy, TILT experiments can be utilized, such as TILT ^{1}H,^{1}H TOCSY-^{1}H,^{13}C HSQC[20, 21]. In the case of very small coupling constants, when the magnetization transfer can not continue around the whole spin system, it can be necessary to combine the above mentioned experiments with NOESY experiments, which are mediated through space, or a ^{1}H,^{13}C HMBC experiment, which is a long-range chemical shift correlation experiment. In pyranoses, the anomeric configuration can be determined from scalar coupling constants ($^{3}J_{H,H}$ and $^{1}J_{C,H}$) and from chemical shifts (^{1}H and ^{13}C).

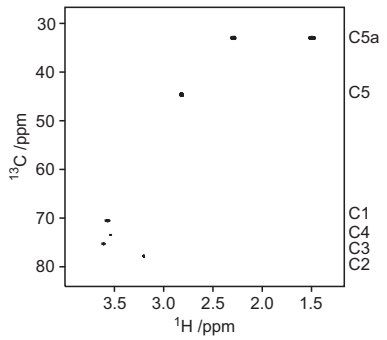

Figure 2.1. HSQC-HT spectrum of the non-methylated carba analogue of iduronic acid discussed in section 4.

After assigning all of the resonances, the linkage positions are investigated. By comparing the chemical shifts of the polysaccharide to the corresponding monosaccharide chemical shifts, glycosylation shifts are obtained. The ^{13}C glycosylation chemical shifts are shifted to 5-10 ppm higher chemical shifts

upon glycosylation.[22] Interresidue NOEs and $^{1}H,^{13}C$ HMBC correlations are used to find the sequence of the sugar residues.

CASPER[23] (Computer-Assisted SPectrum Evaluation of Regular polysaccharides, www.casper.organ.su.se/casper) can be very helpful when elucidating the structure of an oligo- or polysaccharide. It calculates chemical shifts based on the constituent monosaccharides and the glycosylation shifts from substitutions. In the case of a known structure, CASPER can calculate the ^{1}H and ^{13}C chemical shifts and experimental data can be compared to calculated data from CASPER to validate the structure. When the structure is unknown, the carbohydrate sequence can be determined from 1D and/or 2D NMR data by finding the structure with the best agreement between experimental and calculated chemical shifts.

2.3 Conformational studies

When studying the conformation of the glycosidic linkage, two consecutive torsion angles, ϕ and ψ, (three, including ω, in the case of (1→6)-linked disaccharides) are needed to define the conformation of the glycosidic linkage, see *Figure 1.4*. One difficulty in obtaining this information using NMR spectroscopy is that there are no $^{3}J_{H,H}$ values related to the glycosidic torsion angles. Instead these torsions are determined by measuring transglycosidic heteronuclear coupling constants, residual dipolar coupling constants and NOE distances.

2.3.1 Coupling Constants

Scalar coupling constants (*J*-couplings), both homonuclear ($J_{H,H}$ and $J_{C,C}$) and heteronuclear ($J_{C,H}$), are mediated through bonds. The magnitude of the coupling constant is related to geometry by Karplus type relationships.[24]

$$J(\theta) = A\cos^2\theta - B\cos\theta + C$$

where A, B and C are constants and θ is the torsion angle. A single value of the coupling constant corresponds to several torsion angles (*Figure 2.2*), which means that the torsion angle cannot be unambiguously determined by measuring one coupling constant. When different methods are used in combination with each other, *e.g.*, homonuclear and heteronuclear coupling constants, this ambiguity can be avoided and the three-dimensional geometry of a molecule can be found.

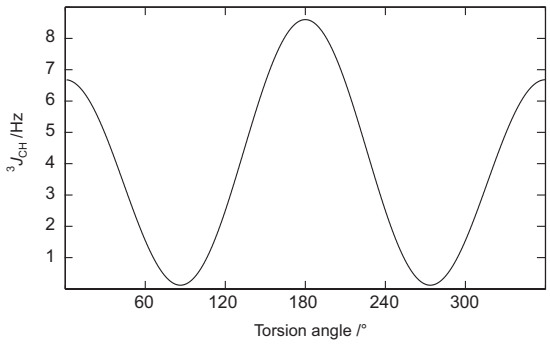

Figure 2.2. Plot of coupling constant as a function of the torsion angle for $^3J_{COCH}$.[25]

Different relationships, in which the coupling path and the electronegativity of substituents are taken in to account, exist for different types of systems.[26] Traditionally Karplus equations are parameterized on the basis of conformationally constrained small molecules with substitutent patterns similar to that of the molecule of interest, or by relating the coupling constant to dihedral angles measured in crystal structures.[27] These approaches have their limitations; model compounds are limited in number and can sometimes have structural strain yielding anomalous torsion angles. More recently computational methods have been used in combination with experimental data to reparameterize Karplus equations.[28]

As a result of the dependence on the Karplus relationship, scalar $^3J_{H,H}$ coupling constants are commonly used to determine 3D-structures of molecules. In many instances scalar $^3J_{H,H}$ coupling constants can easily be extracted from a 1D ^{1}H NMR spectrum. When investigating the conformation of oligosaccharides two types of ^3J-values are related to the glycosidic linkage, $^3J_{C,H}$ and $^3J_{C,C}$. When measuring ^{13}C–^{13}C coupling constants the low abundancy of the ^{13}C nucleus is a problem, and ^{13}C isotopically labeled compounds are required to obtain a sufficient signal to noise ratio.

Heteronuclear long-range ^{13}C–^{1}H coupling constants ($^nJ_{C,H}$) are other very important parameters in the determination of conformations. These coupling constants are hard to determine due to the small size of the couplings (1–10 Hz), the fact that the sign can be either positive or negative and the low sensitivity of the ^{13}C nuclei. As for homonuclear coupling constants, the magnitude of heteronuclear coupling constants can be determined in a 1D-coupled spectrum, but low sensitivity and complex coupling patterns make this difficult. More commonly, heteronuclear coupling constants are determined by different 2D-NMR spectroscopy techniques where both sign and magnitude can be determined.[29] Three examples are the J-HMBC[30], HECADE[31, 32] and IPAP-Hadamard-HSQC-TOCSY [33,34, 35] experiments, see *Figure 2.3*. In the J-HMBC, the small couplings are scaled with a scale factor, κ, in the indirect dimension to overcome problems with low digital resolution. The HECADE experiment is a HSQC-TOCSY experiment with *E*.COSY type cross peaks where the tilt of the cross-peaks in F_2 reveals the relative sign of the coupling

constants. In the IPAP-Hadamard-HSQC-TOCSY experiment spin selective excitation of ^{13}C satellites is used to separate the in-phase and anti-phase components resulting in two spectra where the difference gives the magnitude and the sign of $^{2}J_{C,H}$ and $^{3}J_{C,H}$ coupling constants. A fourth method for measuring $^{3}J_{C,H}$ coupling constants is using the 1DLR experiment published by Nishida *et al.*[36]

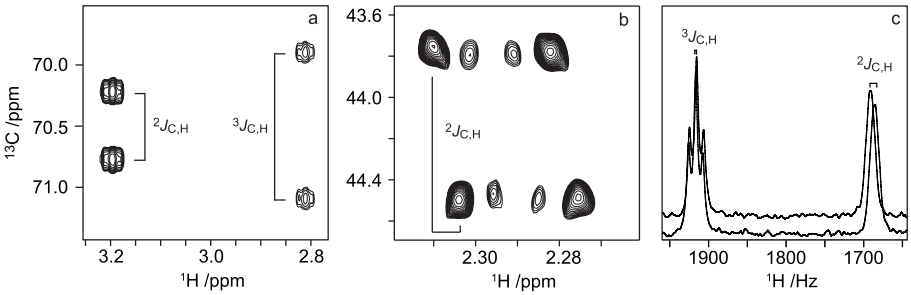

Figure 2.3. a. J-HMBC, b. HSQC-HECADE and c. IPAP-Hadamartd-HSQC-TOCSY spectra of the the non-methylated carbaiduronic acid derivative **2** in paper I.

2.3.2 Spin simulation

When extracting coupling constants and chemical shifts from a one dimensional NMR spectrum, it is not necessarily the true coupling constant that is seen. When the coupling constant is in the same order of magnitude as the chemical shift difference between two coupled nuclei a phenomenon named strong coupling occurs.[17] This is very common when dealing with carbohydrates. If more than two nuclei are present in the spin system, the spectrum becomes complex and it can be hard to extract true coupling constants and chemical shifts by hand. One solution to overcome this problem is to change the magnetic field, naturally this is often not possible. Instead, to be able to measure coupling constants accurately, despite severe overlap and strong coupling effects, NMR spin simulation can be used.[37] A software package that enables this is PERCH (PERCH software, http://www.perchsolutions.com). PERCH is an NMR spectrum prediction and spectral analysis software package. Approximate chemical shifts, coupling constants and an experimental spectrum are used as input data. The program then iteratively fits a calculated spectrum to the experimental. When the two spectra are identical, the true chemical shifts and coupling constants can be extracted. An example of an experimental and a calculated spectrum is shown in *Figure 5.6*.

2.4 Relaxation

Nuclear spin relaxation is the return of magnetization to equilibrium after a perturbation. This process requires loss of energy to magnetic fields oscillating close to the Larmor frequency. The magnetic fields are local and originate from the interactions between spins and between spins and their environment. There are two types of relaxation; longitudinal relaxation and transverse relaxation. Longitudinal relaxation is the recovery of magnetization along the z-axis; this corresponds to the populations returning to equilibrium and is an exponential decay. The time constant of the process is T_1, and the rate constant is the inverse, *i.e.*, $R_1 = 1/T_1$. The classical way to measure T_1 is by an inversion recovery experiment. Transverse relaxation is the loss of magnetization in the xy plane, it is also an exponential decay with T_2 being the time constant and R_2 being the inverse of T_2, *i.e.*, $R_2 = 1/T_2$. T_2 is measured with the CPMG pulse sequence.[17, 38, 39]

The time-dependence of the local magnetic fields originates from the tumbling of the molecule, characterized by a rotational correlation time, τ_c, which is the average time it takes for a molecule to rotate one radian. Thus, short correlation times correspond to rapid tumbling (small molecules) and long correlation times correspond to slow tumbling (large molecules). The regime occupied by small rapidly tumbling molecules is called the extreme narrowing regime. For these systems, the relaxation is slow, *i.e.,* T_1 is long. In the extreme narrowing regime, T_1 and T_2 are equal. For longer correlation times, T_1 becomes large again, but T_2 becomes short, resulting in broad linewidths.

The principle mechanisms by which relaxation takes place are the dipole-dipole, spin rotation and chemical shift anisotropy (CSA) mechanisms. The dipolar mechanism is the most important mechanism for small and medium sized molecules. It originates in the interaction between the local magnetic fields of two spins.

Interaction with an unpaired electron, as in molecular oxygen, can give rise to dipolar relaxation, and for that reason, samples need to be degassed before performing quantitative relaxation measurements. CSA is an important relaxation mechanism for nuclei with large chemical shift range, such as ^{19}F and ^{31}P, but is small for ^{1}H and ^{13}C nuclei in small molecules. For small molecules, and for freely rotating methyl groups, the spin-rotation mechanism is also important.[17, 38, 39]

2.4.1 The model-free approach

To interpret relaxation data with dynamical models, the Lipari-Szabo model-free approach[40] is often used. This analysis can be made with the Modelfree program[41] which uses five different models to fit relaxation parameters, see *Figure 2.4*. As input to the program, relaxation rates, R_1 and R_2, and heteronuclear NOEs at different magnetic fields are used. The relaxation data is

fitted to the different models, and if the model is statistically approved it is used. The model-free approach assumes that the molecule is a perfect sphere and rotates isotropically. All five models calculate the global correlation time, τ_m. Models 4 and 5 are more complex and will not be discussed here. In the simpler models, models 1-3, the generalized order parameter, S^2, is calculated. This gives a value of the flexibility of the system; a value of 0 means a completely flexible system, while 1 means a totally rigid system. For model 1, τ_m and S^2 are the only parameters calculated. In model 2, an additional correlation time is fitted, τ_e, which is an internal correlation time. In model 3 an exchange term, R_{ex}, is also included. From the Lipari-Szabo model-free parameters we can thus get information about the global and local motions of a system from experimental data.

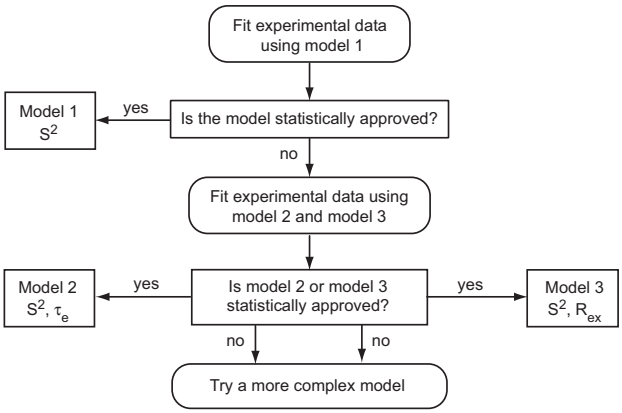

Figure 2.4. Flowchart over the model selection procedure in the Modelfree program.

2.4.2 The nuclear Overhauser effect

The through-space distance between two protons is a useful parameter when determining molecular conformations. By NMR spectroscopy, quantitative measurements of ^{1}H–^{1}H distances are possible via the nuclear Overhauser effect (NOE). When a spin is perturbed (or saturated) away from equilibrium, other spins close in space are affected. The strength of this interaction is dependent on the distance between the protons, the external field (B_0), and the rotation of a molecule, *i.e.*, the correlation time (τ_c). For small molecules, the tumbling is fast and the NOE is positive. For medium size molecules, when $\omega\tau_c$, is close to one, the NOE approaches zero, and becomes negative for large molecules with slow molecular tumbling, see *Figure 2.5*.[17] The rotating frame Overhauser effect (ROE)[17], which is always positive, can be used in instances when the NOE is close to zero. When measuring ROE, a spin-lock is applied. Unfortunately this can lead to magnetization transfer

through bonds (TOCSY-transfer). To avoid TOCSY artifacts, transverse rotating frame Overhauser effect (T-ROE)[42, 43] can be used.

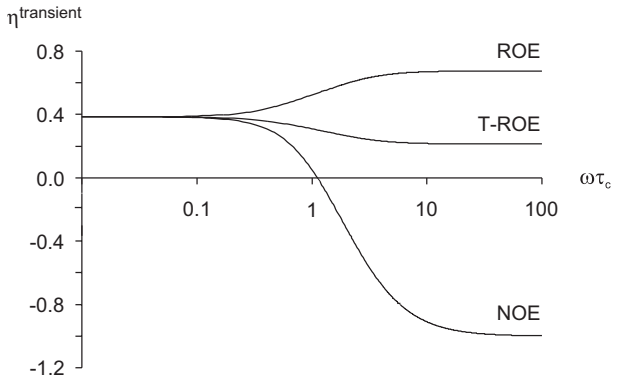

Figure 2.5. The transient NOE effect for NOE, ROE and T-ROE plotted against $\omega\tau_c$.

The NOE signal builds up with time, until a maximum is reached. The initial build-up rate, σ, is proportional to r_{ij}^{-6}, and is related to the distance by the isolated spin pair approximation (ISPA):[44]

$$r_{ij} = r_{ref}\left(\sigma_{ref}/\sigma_{ij}\right)^{1/6}$$

To measure distances, a series of 1D-experiments with selective excitation using different mixing times are collected. The peak area increases with longer mixing times. The cross-relaxation rates can be extracted by two methods; either from a build-up curve where the peak intensities are plotted against the mixing times, or for sufficiently small mixing times, from plotting the peak intensities (I_j) at a certain mixing time (τ_{mix}) divided by the auto-peak intensity (I_i) and the mixing time.

$$\sigma_{ij} = -I_j(\tau_{mix})/[\tau_{mix} I_i]$$

From a series of experiments, a straight line can be plotted and extrapolated to zero. The cross-relaxation rate, σ, can be extracted from this procedure. Cross-relaxation is related to the effective correlation time (τ_{eff}) of a molecule through $\sigma_{NOE}/\sigma_{ROE}$ and $\sigma_{NOE}/\sigma_{T-ROE}$ ratios. A quick estimate of the effective correlation time can be made from *Figure 2.6* where the variations of these ratios are plotted as a function of τ_{eff}.

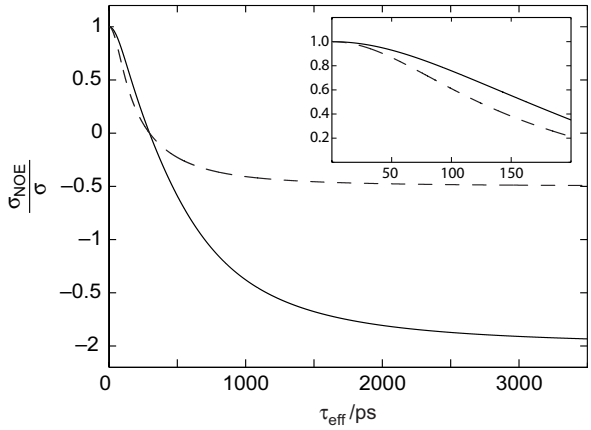

Figure 2.6. σ_{NOE}/σ ratios, where σ is either σ_{ROE} (dashed line) or $\sigma_{T\text{-}ROE}$ (solid line), as a function of τ_{eff} calculated for a 600 MHz magnetic field. The insert shows the behavior up to 200 ps.

2.5 Diffusion

Molecules move randomly in solution. This movement is called diffusion and can be either rotational or translational, see *Figure* 2.7. Translational diffusion is quantified by the diffusion constant, D_t. It can be considered as a random walk or a Brownian motion.

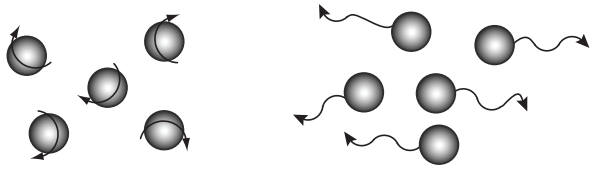

Figure 2.7. Rotational diffusion (left) and translational diffusion (right) for molecules in solution.

The diffusion constant is related to the temperature (T), the viscosity (η) of the solvent and the size and shape of the molecule.[38] In the idealized case of a sphere this relationship is given by the Stokes-Einstein equation;

$$D_t = \frac{k_B T}{6\pi\eta R_H}$$

where k_B is the Boltzmann constant, T is the temperature, η is the viscosity of the solvent and R_H is the hydrodynamic radii. The Debye-Stokes equation relates the hydrodynamic radii to the correlation time, τ_R,

$$\tau_R = \frac{4\pi {R_H}^3 \eta}{3k_B T}$$

The diffusion constant of a molecule can be used to investigate the size and shape of it, to analyse mixtures and impurities of a sample and to study ligand-receptor interactions. NMR spectroscopy is one method of measuring the diffusion of a molecule.[45] It is done by a series of 1D ^{1}H PFG (pulsed field gradient) NMR experiments, in which the overall gradient strength is incremented in each experiment. Two gradient pulses are applied, and during the time between the pulses, the diffusion time (Δ), the molecules move randomly and the local field experienced by the molecule is not exactly the same after the second gradient pulse. The signal will be attenuated since it is not fully refocused. Smaller molecules move faster and will experience more difference in the local field giving a greater attenuation of the NMR signal.[38] The NMR signal echo intensities are plotted on a logarithmic scale *vs.* $(\gamma\delta g)^2(\Delta - \delta/3)$, according to the Stejskal-Tanner equation[46];

$$A = A_0 \exp\left[-(\gamma\delta g)^2(\Delta - \delta/3)D_t\right]$$

where A_0 is the amplitude when no gradients are used, γ is the magnetogyric ratio of the nucleus, δ is the length of the gradient pulse, g is the gradient strength, and Δ is the time separation between the gradient pulses. In the logarithmic plot, the diffusion coefficient is extracted from the slope.

3 Molecular dynamics simulations

Molecular dynamics (MD) simulation is a valuable tool in the study of carbohydrates and other biomolecules. In contrast to NMR spectroscopy, where a time average of motions is seen, in MD simulations these motions can be studied on a shorter time scale. In an MD simulation, molecules are allowed to move and interact over a period of time. The molecular motions are calculated by solving Newton's second law of motion. To mimic nature as much as possible, the system can be solvated, usually in water. This addition of water molecules makes the calculations very time-consuming. To make the simulation more efficient, periodic boundary conditions, where the model system is surrounded by images of itself, are used. A force field is applied to the system during the MD simulation to describe the potential energy of the system. A general form of the total energy can be described as:

$$E_{total} = E_{bond} + E_{angle} + E_{dihedral} + E_{improper} + E_{non-bonded}$$

The results from MD simulations are only as good as the force field used; thus, the choice of force field is crucial to the outcome of the MD simulation. In this work the PARM22/SU01 force field[47,48] modified for carbohydrates, has been used. New and refined force fields are constantly under development, and one example is a recently published CHARMM additive force field.[48, 49]

Information from a molecular dynamics simulation can be used to map the conformational space of a molecule. A trajectory of a variable, such as atom–atom distances or a torsion angle as a function of time is often created. These variables can be compared to experimental data, for example, NOE derived distances and *J* couplings. The combination of simulated data and experiments is very powerful and can give much information about a system.[50]

4 Synthesis and conformational analysis of carbasugar isosteres of α-L-iduronic acid and its methyl glycoside (paper I)

4.1 Introduction

Idose and iduronic acid (Ido*p*A) are unusual among hexoses in that their pyranose forms do not exist exclusively in a single chair conformation. On the contrary, they are rather flexible, having several low-energy conformations.[12] Iduronic acid is a component of various biologically active glycans, such as the glycosaminoglycans heparin, heparan sulfate and dermatan sulfate. These structures are unbranched and consist of repeating units of an amino sugar and a (1→4)-linked L-uronic acid, α-linked in the case of L-iduronic acid and β-linked in the case of D-glucuronic acid. One important role of heparin is its anti blood-clotting property, which is due to its binding to the protein anithrombin III. The minimal effective structural element in heparin binding has been identified as a pentasaccharide fragment.[1] Ferro *et al.* have proposed that the flexible nature of iduronic acid is the key to the strong binding to antithrombin.[12]

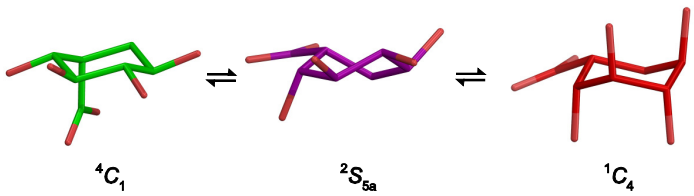

*Figure 4.1.*The three proposed low-energy conformations of the carba analogs of L-iduronic acid.

As mentioned in section 1.3, iduronic acid exists in three low-energy conformations, $^4C_1$, ^2S_O and, $^1C_4$ shown in *Figure 1.3*. Calculations of α-L-Ido*p*A show that the $^1C_4$ conformation is the most energetically stable with a small contribution of the $^4C_1$ conformation.[51, 52] If α-L-Ido*p*A is situated internally in oligosaccharides related to heparin, it will only populate the $^1C_4$ and ^2S_O conformations, whereas non-sulfated α-L-Ido*p*A situated as a terminal group also populate the $^4C_1$ conformation.[53] From the study of different conformationally locked mimics of iduronic acid and the active pentasaccharide, it has

been shown that the skew-boat, $^{2}S_{O}$, conformation is required for binding to antithrombin.[54, 55]

Carbasugars are carbohydrate analogs in which the endocyclic oxygen has been replaced by a methylene group. This means that the acetal linkage of a glycoside is formally transformed into an ether for a carbasugar, and hence becomes hydrolytically stable.[56, 57] Two carbaiduronic acid derivatives were synthesized as hydrolytically stable mimics of iduronic acid, namely the α-analogue **2** and the 1-*O*-methyl ether derivative **3**, starting from the cyclohexene derivative **1**[58], shown in *Figure 4.2*.

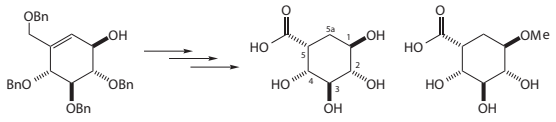

1 2 3

Figure 4.2. The two carbaiduronic acid derivatives **2** and **3**, and the starting compound **1**. The numbering used herein is shown in compound **2**.

The scope of this study was to investigate the ring conformation of these two synthetic carba-analogues of α-L-Ido*p*A. The equilibrium between three different conformations, $^{4}C_{1} \leftrightarrows {}^{2}S_{5a} \leftrightarrows {}^{1}C_{4}$, was considered in this study, see *Figure 4.1*. These are the same conformations that are present in the natural occurring compound α-L-Ido*p*A.

4.2 Conformational studies

The conformational analysis of the two carbaiduronic acid derivatives is based on NMR spectroscopy and molecular modeling. Chemical shift assignment of **2** and **3** was achieved from 1D ^{1}H and ^{13}C NMR spectra and from 2D methods such as ^{1}H,^{13}C HSQC-HT[34], (see *Figure 2.1*) ^{1}H,^{1}H TOCSY and ^{1}H,^{13}C HMBC.

The conformation of the six-membered rings was investigated with different NMR techniques. Scalar coupling constants and NOE-distances were used. In this thesis the conformation of only one of the carbaiduronic acids will be discussed, the non-methylated compound **2**. Coupling constants and effective distances were derived for both compounds and the results are very similar for **2** and **3**.

Table 4.1. ^{1}H and ^{13}C chemical shifts in ppm and coupling constants in Hz of the ring atoms.

		1	*2*	*3*	*4*	*5*	*5a-R*	*5a-S*
		$^{3}J_{H1,H2\ /\ H5a\text{-}R\ /\ H5a\text{-}S}$	$^{3}J_{H2,H3}$	$^{3}J_{H3,H4}$	$^{3}J_{H4,H5}$	$^{3}J_{H5,H5a\text{-}R/\ H5a\text{-}S}$	$^{2}J_{H5,H5a\text{-}S}$	
2	^{1}H	3.56	3.20	3.60	3.53	2.81	1.49	2.29
	$J_{H,H}$	9.34, 11.94, 4.67	9.30	9.78	5.57	4.95, 2.97	−13.54	
	^{13}C	70.5	78.0	75.2	73.6	44.1	32.0	
3	^{1}H	3.267	3.274	3.61	3.53	2.84	1.34	2.50
	$J_{H,H}$	9.57, 11.43, 4.36	9.33	9.71	5.54	4.72, 3.10	−13.44	
	^{13}C	80.3	76.7	75.4	73.5	43.8	28.4	

Due to the dependence on the Karplus relationship, $^{3}J_{H,H}$ coupling constants are commonly used parameters to determine 3D-structures and conformations in solution. Homonuclear coupling constants are sensitive to strong coupling effects. The two monosaccharide derivatives studied are very strongly coupled. In compound **3** the protons on carbons 1 and 2 are separated by 0.007 ppm and have a coupling of 9.57 Hz, *i.e.* $\delta_{Hz}/J = 0.5$ at 700 MHz ^{1}H frequency. To be able to extract the true coupling constants, spin simulation with the PERCH NMR software[37] was performed. The coupling constants are presented in *Table 4.1*. In *Figure 4.3* a comparison between the experimental spectra and predicted spectra for the three different ring conformations is shown. The predictions were made for energy-minimized models and the experimental chemical shifts were used as input data. For a comparison of the chemical shifts see *Figure 3* in Paper I. A closer look at a few of the coupling constants for compound **2** indicates a shift of the conformation to the $^{4}C_1$ ring conformation. One example is $^{3}J_{H1,H5a\text{-}R} = 11.94$ Hz, where a large coupling constants can only be explained by a torsion angle close to 180º. When measuring the torsion angle H1−C1−C5a−H5a-*R* in energy minimized structures of the three different conformations, the result is $^{4}C_1 = -174º$, $^{2}S_O = -78º$ and $^{1}C_4 = -64º$. This torsion angle most resembles the $^{4}C_1$ conformation. Furthermore, $^{3}J_{H1,H2} = 9.34$ Hz and $^{3}J_{H3,H4} = 9.78$ Hz also suggest the $^{4}C_1$ conformation. For the two other conformations these coupling constants would be around 3 Hz.

As discussed in section 2.3.1, heteronuclear long-range coupling constants can give valuable information about conformation. Three different NMR techniques were utilized to unambiguously extract these parameters. The three methods, J-HMBC[30], HSQC-HECADE[31, 32] and IPAP-Hadamard-HSQC-TOCSY[33, 35, 59, 60], are all two-dimensional heteronuclear experiments and are discussed in more detail in section 2.3.1. NMR spectra resulting from the three experiments are shown in *Figure 2.3*, the heteronuclear coupling constants are presented in Table 2 in paper I. The quantified coupling constants were consistent between the three experiment types within the experimental error of ±0.5 Hz.

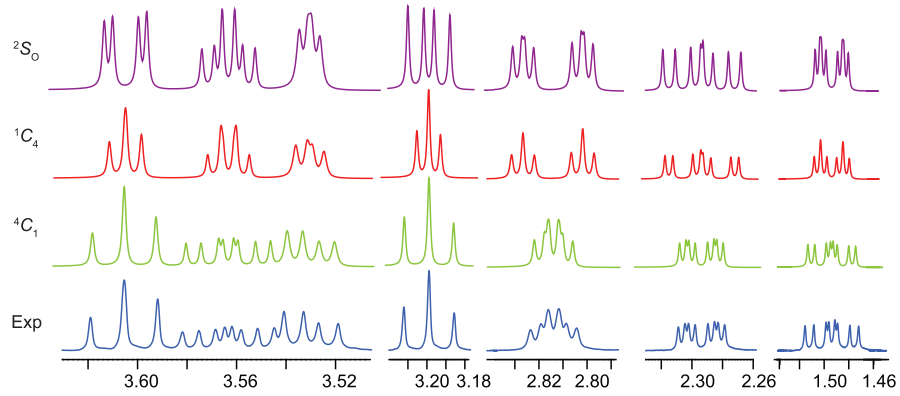

Figure 4.3. Comparison of experimental and predicted $J_{H,H}$ coupling constants at 700 MHz for compound **2**. Experimental chemical shifts were used as input for the spectra predictions of the three conformations.

As for the homonuclear coupling constants, the measured heteronuclear coupling constants were compared to what is expected from energy minimized models of the three conformations. The Karplus type relationship proposed by Wasylishen and Scaefer[61] was used to calculate heteronuclear coupling constants.

$$^3J_{C,H} = 4.26 - 1.00 + 3.56\cos 2\theta$$

Two examples are $^3J_{C3,H5}$ = 8.3 Hz and $^3J_{C2,H5a\text{-}R}$ = 2.8 Hz, the first must be related to a torsion angle close to 180º while the second corresponds to a torsion angle close to 90º, this is again only possible in the case of the $^4C_1$ conformation. A comparison of the fitted coupling constants from PERCH with the calculated values for the energy-minimized structures of the three conformations is shown in *Figure 4.4*.

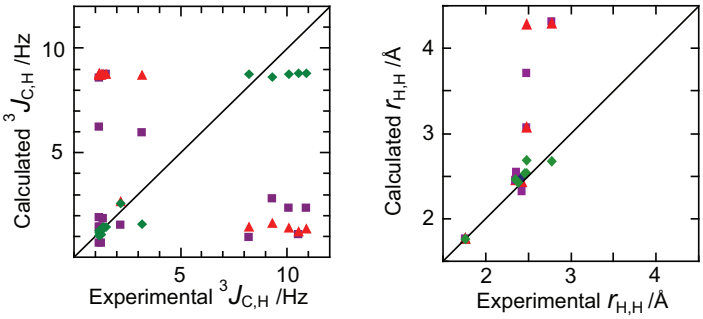

Figure 4.4. Comparison between experimental values, $^3J_{C,H}$ (left), and r_{eff} (right) and calculated values from energy-minimized models. $^4C_1$ (green diamonds), $^2S_{5a}$ (purple squares) and $^1C_4$ (red triangles). To the left $^3J_{C,H}$ is shown and to the right ^{1}H,^{1}H distances are shown.

Additional information about the ring conformations for the two carbaiduronic acid analogs was obtained from 1D ^{1}H,^{1}H NOE and 1D ^{1}H,^{1}H T-ROE measurements. Three protons were selectively excited, the H5a-*R*, H5a-*S* and H5. As reference distance H5a-*R*–H5a-*S* = 1.79 Å was used. The two measurements are in good agreement with each other. In *Table 4.2* the experimental effective distances are compared to theoretical distances from the three different conformations. The experimentally determined distances between H5a-*R*–H2 and H5–H5a-*S* are again only possible in the $^4C_1$ conformation.

Table 4.2. Effective distances from NMR experiments and calculated distances from Molecular Mechanics optimized structures for **1**.

Atom pair		NMR r_{eff} /Å		Molecular Mechanics r_{eff} /Å		
		T-ROE[a]	NOE[a]	$^4C_1$	$^2S_{5a}$	$^1C_4$
H5	H4	2.38	2.38	2.43	2.45	2.45
H5	H5a-*R*	2.35	2.35	2.46	2.54	2.47
H5	H5a-*S*	2.47	2.46	2.53	3.06	3.07
H5a-*R*	H2	2.50	2.47	2.68	3.70	4.28
H5a-*R*	H5a-*S*	1.76[b,c]	1.76	1.76	1.76	1.76
H5a-*S*	H1	2.42	2.43	2.48	2.32	2.43

[a]Selective excitation of the first resonance in the atom pair. [b]Average values from excitation of both resonances in the atom pair. [c]Reference distance.

Based on the results presented, ^{1}H chemical shifts, homo- and heteronuclear coupling constants and effective proton-proton distances, it is clear that the $^4C_1 \leftrightarrows {}^2S_{5a} \leftrightarrows {}^1C_4$ equilibrium is shifted towards the $^4C_1$ conformation. This conformation is the predominant or exclusive conformation. An increase in the $^2S_{5a}$ or $^1C_4$ conformations would not lead to better agreement with the experimental data. When the ring oxygen in α-L-Ido*p*A is exchanged for a methylene group the anomeric effect is no longer present. The anomeric effect stabilizes the conformation where the C1–O1 bond is axial, *i.e.* the $^1C_4$ conformation. The carbaiduronic acid derivatives investigated in this study could still be suitable as hydrolytically stable residues in synthetic oligosaccharides. As mentioned in the introduction, the conformational equilibrium might change if the monosaccharides are internal in an oligosaccharide sequence or if they are sulfated.

4.3 Conclusions

Homo- and heteronuclear coupling constants in combination with proton-proton distances were used to study the conformation of the carbaiduronic acid derivatives. When comparing measured homonuclear and heteronuclear coupling constants and NOE distances to theoretical values from energy minimized molecular models, it is clearly seen that the $^4C_1$ conformation is

dominant. The conformations of the derivatives studied here do not exhibit the conformational flexibility that has been found in the natural analogs in oligo- and polysaccharides. The results are very similar for the two carbasugars.

Three different NMR experiments were used to measure heteronuclear coupling constants; the agreement between them was good. By combining these different methods, most coupling constants can be resolved even in very crowded carbohydrate NMR spectra. The study shows that the ring conformation of six-membered rings can be thoroughly investigated with different NMR techniques.

To be able to use carbasugars as hydrolytically stable mimics in pseudo-oligosaccharides, the conformation of sulfated analogs of carbasugars incorporated into heparin-like oligosaccharides should be studied. The different environment could alter the conformational equilibrium as has been seen for iduronic acid.

5 Conformational flexibility and dynamics of two (1→6)-linked disaccharides related to an oligosaccharide epitope expressed on malignant tumor cells (paper II)

5.1 Introduction

Malignant tumor cells are known to have large highly β-(1→6) branched complex *N*-glycans present on the cell surface.[62] These glycans result from an over-expression of the protein N-acetylglucosylaminyl transferase V (GnT-V). GnT-V increases the branching of *N*-glycans by adding a GlcNAc residue to the core of an *N*-glycan, see *Figure 5.1*[63]. The GlcNAc is added to position 6 in an α-D-Man*p* fragment, forming a β-D-Glc*p*NAc-(1→6)-α-D-Man*p* linkage. A trisaccharide, β-D-Glc*p*NAc-(1→2)-α-D-Man(1→6)-β-D-Man*p*, is required as an acceptor to GnT-V and UDP-GlcNAc is needed as a donor.[63]

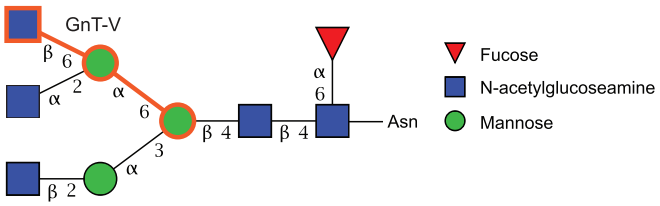

Figure 5.1. Schematic in CFG notation of a complex type *N*-glycan with the trisaccharide of interest highlighted with orange frames.

It has previously been shown that the ω-conformation of the acceptor trisaccharide is important. If the conformation of the acceptor is shifted towards the *gt* rotamer it is more active and if it is shifted towards the *gg* rotamer it is less active than the non-perturbed acceptor.[64] The importance of the increased branching of *N*-glycans on malignant cells is known; however, the mechanism of how the structure is related to cancer is not fully understood. Therefore, we wanted to study the conformational dynamics of mono- and disaccharide fragments related to the trisaccharide acceptor in detail. Chemically synthesized [6-^{13}C] site-specifically labeled analogs were studied using a range of NMR spectroscopy experiments. Molecular dynamics simulations

were used to generate a model to be compared with the NMR spectroscopy results and to describe the conformational dynamics of the fragments.

5.2 Conformational studies

The conformational dynamics of three compounds related to branched *N*-glycan structures were investigated in this study, namely α-D-Man*p*-OMe (**1**), β-D-Glc*p*NAc-(1→6)-α-D-Man*p*-OMe (**2**) and α-D-Man*p*-(1→6)-α-D-Man*p*-OMe (**3**), shown in *Figure 5.2*. The analysis of the fragments in question was facilitated by site-specific ^{13}C labeling at position 6 in the glycosidic linkage, highlighted in *Figure 5.1*. The compounds were synthesized both with and without ^{13}C labeling. For α-D-Man*p*-OMe and α-D-Man*p*-(1→6)-α-D-Man*p*-OMe, mainly the ω torsion angle was studied while β-D-Glc*p*NAc-(1→6)-α-D-Man*p*-OMe was investigated in more detail.

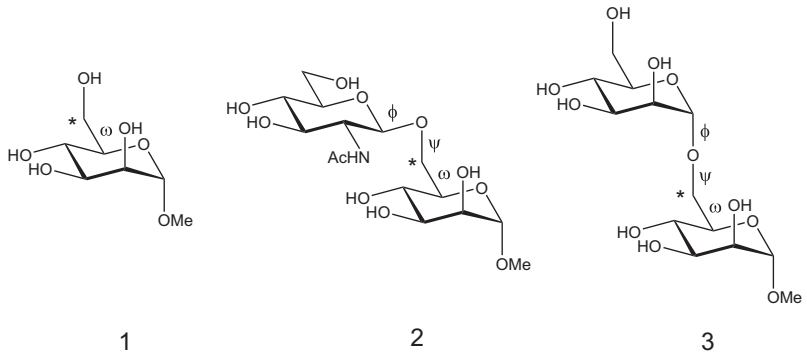

Figure 5.2. α-D-Man*p*-OMe (**1**), β-D-Glc*p*NAc-(1→6)-α-D-Man*p*-OMe (**2**) and α-D-Man*p*-(1→6)-α-D-Man*p*-OMe (**3**) with the selectively labeled carbon marked with an asterisk.

In hexopyranosides, the population of the three staggered conformers of the ω torsion angle, *gt, gg* and *tg,* can be experimentally determined from the $^3J_{H5,H6}$ coupling constants according to Stenutz *et al.*[65] In *Table 5.1*, a summary of the experimentally determined coupling constants are listed as well as the calculated population distributions between the three ω conformations. The population distributions were calculated in three ways; from NMR coupling constants, from MD simulations and from data extracted from the Protein Data Bank. The $^2J_{C4,C6}$ and $^2J_{C6,H5}$ coupling constants are also related to the ω torsion angle and can be used when determining the rotamer distribution.[66] For $^2J_{C4,C6}$, the coupling constants are small for all three rotamers (*gg*: 1.3 Hz, *gt*: −1.1 Hz and *tg*: −0.1 Hz), while for $^2J_{C6,H5}$ the difference between the rotamers is much larger (*gg*: +2.7 Hz, *gt*: −3.7 Hz and *tg*: −2.8 Hz).

Table 5.1. $^{3}J_{H,H}$ and $^{2}J_{C,H}$ coupling constants and ω rotamer distributions for the ^{13}C labeled compounds **1** – **3** and structures present as part of glycoproteins in crystal structures.

Compound	$^{3}J_{H5,H6\text{-}R}$ /Hz	$^{3}J_{H5,H6\text{-}S}$ /Hz	$^{2}J_{C6,H5}$ /Hz	*gt* /%	*gg* /%	*tg* /%
α-D-Man*p*-OMe	6.14 [0.06][a]	2.23 [0.04]	-1.98 [0.03]	55 (44)[b]	36 (38)	9 (18)
β-D-Glc*p*NAc-(1→6)-α-D-Man*p*-OMe	6.48 [0.21]	1.91 [0.05]	-2.15 [0.04]	60 (67)	35 (28)	5 (5)
α-D-Man*p*-(1→6)-α-D-Man*p*-OMe	5.12 [0.12]	1.96 [0.26]	-1.69 [0.22]	45	50	5
α-D-Man*p*-(1→6)-D-Man*p*-(1→[c]				40	55	5

[a]Standard deviation from NMR spin simulation at four different magnetic fields. [b]Populations calculated from the MD simulations are given in parentheses. [c]Populations calculated from the occurrences in the Protein Data Bank.

To avoid problems with strong coupling effects and to overcome problems with spectral overlap, all coupling constants, except for ^{13}C-^{13}C coupling constants, presented were extracted and refined with spin simulation of 1D-^{1}H NMR spectra at four different fields (400 MHz, 500 MHz, 600 MHz and 700 MHz) using the PERCH NMR software. At 600 MHz and 700 MHz, ^{1}H and coupled ^{13}C NMR spectra were combined to one spectrum and simulated at the same time. The signs of the $^{2}J_{C6,H5}$ coupling constants were verified by HSQC-HECADE experiments.

The non-substituted α-D-Man*p*-OMe (**1**) was used as a reference compound in the analysis of the ω-torsion angle. A 40 ns long molecular dynamics simulation was performed using explicit water as solvent. The force field used in this study was the CHARMM based force field PARM22/SU01[47]. From the molecular dynamics simulation, the population distribution of the ω torsion angle is 44% *gt*, 38% *gg* and 18% *tg*. The results for α-D-Man*p*-OMe from the MD simulation are in good agreement with the distribution calculated from the H5–H6 coupling constants, 55% *gt*, 36% *gg* and 9% *tg*. This distribution is expected from the gauche effect and the Hassel-Ottar effect. From this we can conclude that the force field describes the ω torsion angle well and that it can be used to describe the ω distribution for compound **2** as well.

A 25 ns long MD simulation in explicit water of β-D-Glc*p*NAc-(1→6)-α-D-Man*p*OMe (**2**) was performed. Analysis of the ω torsion angle showed a rotamer distribution slightly different from that of compound **1**. The *gt* conformation is more populated with 67% while the *gg* rotamer decreases to 28%, and *tg* (5%) still has a small population. This is in agreement with a previous study.[67] The H5–H6 coupling constants gave the distribution 60:35:5, well in agreement with the MD simulation.

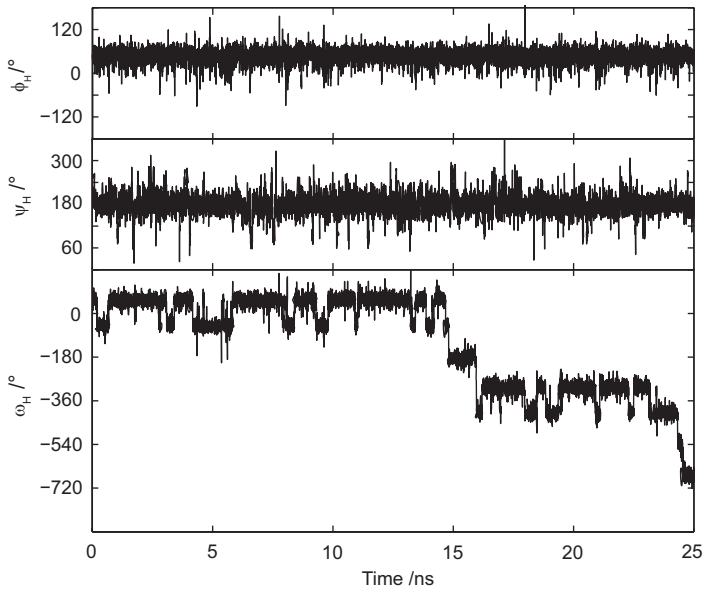

Figure 5.3. Trajectory plots of the 25 ns long simulation of β-D-Glc*p*NAc-(1→6)-α-D-Man*p*-OMe (**2**), show that ϕ and ψ mainly exist in one conformation while all three conformations are populated for ω.

For β-D-Glc*p*NAc-(1→6)-α-D-Man*p*-OMe, the ϕ and ψ torsion angles were also analyzed in the MD-simulation (*Figure 5.3*). Both torsion angles exist predominantly in one conformation. For ϕ the stabilizing effect is the *exo*-anomeric effect giving a average torsion angle of ϕ = 47°. The heteronuclear coupling constant $^{3}J_{H1',C6}$ = 4.08 Hz is related to the ϕ torsion angle and indicates that the *exo*-anomeric conformation is dominating[68].[68] ψ is slightly more flexible, the average value for the torsion angle is 178°. This *anti*-periplanar arrangement is populated to more than 95% even though it is clear from *Figure 5.3* that the conformations when ψ < 120º and > 300º are populated to a small extent.

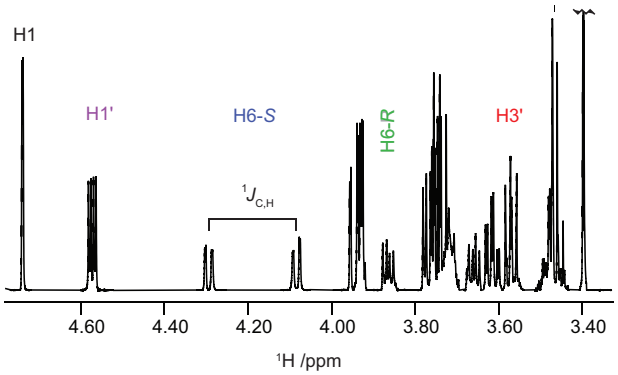

Figure 5.4. Spectrum at 700 MHz of the ^{13}C-labeled disaccharide β-D-Glc*p*NAc-(1→6)-α-D-Man*p*-OMe. The one-bond $J_{C,H}$ splitting can clearly be seen for H6-*S* and one half of H6-*R* has moved out from the crowded region.

To further examine the conformation around the glycosidic linkage, inter-proton distances were measured with 1D ^{1}H,^{1}H NOESY and T-ROESY experiments. H1' was selectively excited and it was possible to extract cross-relaxation rates to H3', H6-*S* and H6-*R*. The measurements were performed on the ^{13}C-labeled compound. The ^{13}C labeling of C6 splits the H6 protons with the $^1J_{C,H}$ coupling constant making the half of H6-*R* with higher chemical shift resolved (*Figure 5.4*). Five different mixing times, $\tau_m \leq 200$ ms, were used and cross-relaxation rates were extracted as described in section 2.4.2 by extrapolation to $\tau_m = 0$, see *Figure 5.5*. It can be noted that the slopes differ for the protons that are directly attached to a ^{13}C-labeled carbon, compared to those attached to a ^{12}C.

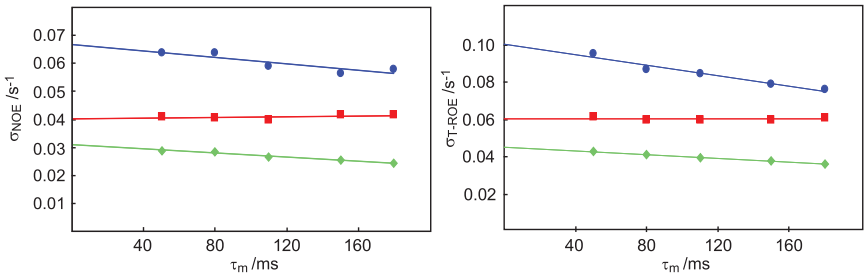

Figure 5.5. Plots of cross-relaxation for the 1D ^{1}H,^{1}H NOESY (left) and T-ROESY (right) experiments for the selectively labeled compound **2**. Selective excitation of H1' in **2** gave correlations to H6-*R* (blue circles), H6-*S* (green diamonds) and H3' (red squares) which were investigated.

The effective correlation times for the three protons were calculated using the ratio of $\sigma_{NOE}/\sigma_{T\text{-}ROE}$ (see section 2.4.2), giving $\tau_{eff} \sim 120$ ps for all three protons (see *Table 5.2*). This means that H3' can be used as a reference when calculating effective proton distances to H6-*S* and H6-*R* with the isolated spin-pair approximation, ISPA. The effective distances are summarized in

Table 5.2. It can be noted that the distance from H1−H6-*R* is shorter than H1−H6-*S*, also this in good agreement with the MD simulation.

Table 5.2.Cross-relaxation rates and effective distances of β-D-Glc*p*NAc-(1→6)-α-D-Man*p*-OMe from selective excitation of H1′ using 1D NOESY and T-ROESY experiments.

Proton detected	σ_{NOE} /$\times 10^2 s^{-1}$	$\sigma_{T\text{-}ROE}$ /$\times 10^2 s^{-1}$	$\sigma_{NOE}/\sigma_{T\text{-}ROE}$	τ_{eff}/ps	$\sigma_{ij}/\sigma_{H3'}$ T-ROE	r_{ij} /Å NMR	r_{ij} /Å MD
H6-*R*	6.67	10.1	0.660	124	1.67	2.33	2.39
H3'	4.01	6.06	0.662	124	1	2.54[a]	2.54
H6-*S*	3.08	4.51	0.683	119	0.744	2.67	2.74

[a]Reference distance from the MD simulation of 25 ns.

A high population of the *exo*-anomeric conformation for ϕ has previously been reported.[69-71] However, for ψ it has been suggested that the conformation of ψ = 180 is only a 'virtual' conformation, being an equilibrium between two different conformations, ψ ~ 90º and ψ ~ 250º. From the experimental and simulated data presented here it looks like this 'virtual' conformation is really the predominant conformation.

For the second disaccharide in this study, α-D-Man*p*-(1→6)-α-D-Man*p*-OMe (**3**), the conformational equilibrium between the *gt* and *gg* rotamers is shifted compared to the two previous examples, *Table 5.2*. The *gg* conformation is, according to the $^3J_{H5,H6}$ coupling constants, populated to 50%, being the most populated of the rotamers. These observations are not in agreement with what has been reported by Spronk *et al.*[72] where $^3J_{H5,H6\text{-}S}$ = 1.9 Hz and $^3J_{H5,H6\text{-}R}$ = 2.2 Hz.

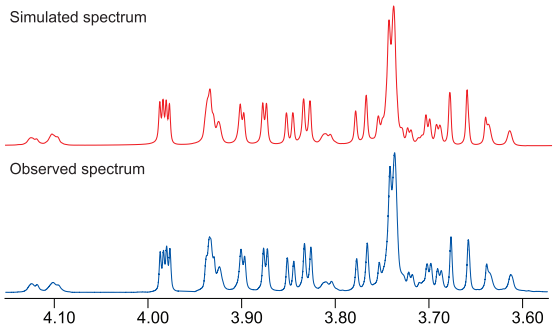

Figure 5.6. Experimental (bottom) and simulated (top) spectra of the ring region of α-D-Man*p*-(1→6)-α-D-Man*p*-OMe (**3**) at 500 MHz.

From the iterative PERCH spin simulation of **3** (*Figure 5.6*), the coupling constants are $^3J_{H5,H6\text{-}S}$ = 1.89 Hz and $^3J_{H5,H6\text{-}R}$ = 5.10 Hz. The two-bond heteronuclear coupling constant $^2J_{C6,H5}$ was spin-simulated from a coupled ^{13}C spectrum and a ^1H spectrum together, the sign of the coupling constant was confirmed by a from a HSQC-HECADE experiment. This coupling constant

($^2J_{C6,H5} = -1.69$ Hz) was compared to theoretical coupling constants[66] for the three different rotamer conformations, see above. Thus, it is clear that the conformation can not exist almost exclusively (96%) as *gg*, as has been suggested.

For all three compounds the $^2J_{C4,C6}$ is vanishingly small (<0.5 Hz) and $^2J_{C6,H5}$ has a negative sign, see *Table 5.1*. When the *tg* rotamer is only marginally populated, as shown for all three cases, these two coupling constants are dependent on an equilibrium between the *gt* and *gg* conformations. Also, the negative signs of the $^2J_{C6,H5}$ coupling constants confirm the finding that the ω distributions are similar in all three molecules.

A number of *N*-linked glycoproteins have been reported in the protein data bank (PDB). With the program GLYTORSION[16] it is possible to extract information about the carbohydrate part of the proteins. 218 crystal structures containing α-D-Man*p*-(1→6)-α/β-D-Man*p* linkages, with a resolution <2.5 Å, were analyzed. A distribution of 40% *gt*, 55% *gg* and 5% *tg* was obtained, which is very close to what was observed experimentally in solution. This indicates that the conformational preference is retained in the solid state.

5.3 Conclusions

The models obtained from MD simulations with the force field PARM22/SU01 in this study were found to be in excellent agreement with the experimental data obtained for both α-D-Man*p*-OMe and β-D-Glc*p*NAc-(1→6)-α-D-Man*p*-OMe. The flexible and dynamic ω torsion angle was well described by the force field. Experimental transglycosidic distances and coupling constants were in agreement with the MD simulations.

The use of spin-simulations at different fields, and ^{1}H NMR spectra combined with ^{13}C NMR spectra, proved to be very useful for accurately extracting $J_{H,H}$ and $J_{C,H}$ coupling constants. Site-specific ^{13}C labeling is powerful in oligosaccharide analysis. It can simplify spectra by increasing the spectral dispersion, and make it possible to extract additional coupling constants.

For α-D-Man*p*-(1→6)-α-D-Man*p*-OMe, we have found that the rotamer distribution is shifted from what has previously been described. Furthermore, it was found that the conformational preference both in solution and in crystal structures is nearly identical. This method of getting additional experimental data can be very useful in studies of the conformational preferences of oligosaccharides.

In the future it would be interesting to extend this study to also include the whole trisaccharide fragment in question and to investigate if the conformational preferences we have found in this study will change in a larger structure. The methods presented here should be suitable also for the larger trisaccharide, even though problems with spectral overlap might make the

study difficult. The use of site-specific labeling and spin-simulation could come in very handy to make it possible to accurately extract coupling constants also in this case.

6 Population distribution of flexible molecules from maximum entropy analysis using different priors as background information: application to the ϕ,ψ-conformational space of the α-(1→2)-linked mannose disaccharide present in *N*- and *O*-linked glycoproteins (paper III)

6.1 Introduction

Proteins often contain one or several oligosaccharide side chains that carry biological information in their three-dimensional structure. The carbohydrate parts are conjugated to proteins as *N*-linked or *O*-linked derivatives. D-Mannose residues are very common in all of these glycoproteins. In *N*-linked glycoproteins it is found as α-(1→2), α-(1→3) and α-(1→6) epitopes. The fragment α-D-Man*p*-(1→2)-α-D-Man*p* in these elements is part of carbohydrate structures recognized by lectins and antibodies.[73, 74] In this study we wanted to investigate the conformational space and the flexibility of the disaccharide α-D-Man*p*-(1→2)-α-D-Man*p*-OMe (M2M), see *Figure 6.1*.

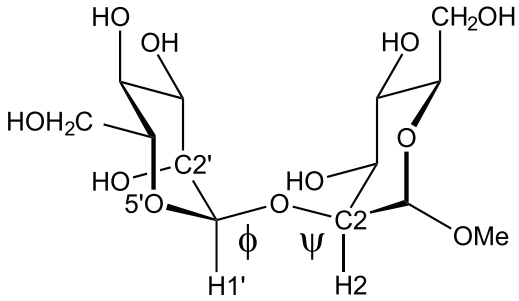

Figure 6.1. Structure of the disaccharide α-D-Man*p*-(1→2)-α-D-Man*p*-OMe, M2M, with the atoms important for the coupling constant pathways explicitly highlighted.

As discussed in previous chapters, oligosaccharides are flexible molecules and two or more conformations are anticipated. The determination of the

population distribution of the different conformations is a problem with more unknowns than experimental data. There is, however, information of preferred and disallowed conformations based on knowledge of, for example, steric interactions and the *exo*-anomeric effect. This information is incorporated in force fields modified for carbohydrates.[47, 48] The results from simulations may still differ significantly between different force fields and between simulations and experimental data; it can be difficult to interpret the results when data from various experiments are compared.

In this work, NMR data for α-D-Man*p*-(1→2)-α-D-Man*p*-OMe was interpreted with background information from either a molecular dynamics (MD) simulation or a database survey (DB) by the maximum entropy (ME) formalism. The background information was used to formulate a hypothesis about the conformational preferences, a *prior*, before the experimental data was considered. After considering the experimental data, a model referred to as a *posterior*, was formed. Both posteriors showed deviations that were not anticipated from the priors. Therefore, we carried out reparameterizations of the corresponding Karplus equations, taking into account the importance of electronegative substituents in the coupling pathway.

The specific torsion angles are defined as follows: ϕ_H = H1′-C1′-O2-C2, $\phi_{O5'}$ = O5′-C1′-O2-C2, ψ_H = H2-C2-O2-C1′ and ψ_{C1} = C1-C2-O2-C1′. The relationship in M2M between the different torsion angles are given by: $\phi_H = \phi_{O5'} - 120°$ and $\psi_H = \psi_{C1} + 120°$.

6.2 Results and discussion

6.2.1 MD simulation

The conformational preference for M2M was first investigated by an MD simulation using the PARM22/SU01 force field.[47] A 21.6 ns long simulation, using explicit water as a solvent, was performed. Three regions were significantly populated, see *Figure 6.2*. For two of them ϕ_H is present in the *exo*-anomeric conformation and ψ_H is positive or negative. The third region has the non-*exo*-anomeric conformation for ϕ_H, and positive values for ψ_H. This population distribution was used as background information for the ME analysis and is referred to as the MD-prior.

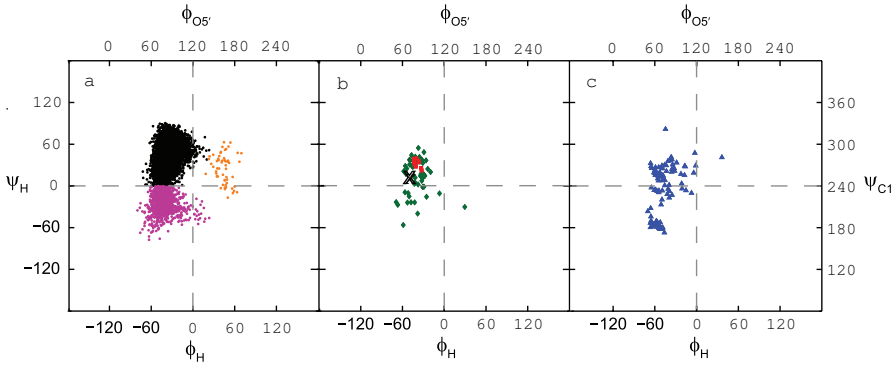

Figure 6.2. Scatter plots of ϕ *vs.* ψ for M2M; (a) from MD simulations, (b) from crystal structures of *O*-linked glycans(red), ligands (green) and (c) *N*-linked glycans having the structural element α-D-Man*p*-(1→2)-α-D-Man*p*. The crystal structure of M2M is denoted as a black cross.

6.2.2 PDB analysis

As shown in paper II, data from the protein data bank (PDB) can be used to gain knowledge of the conformational distribution of the ω-torsion angle. The distributions for the glycosidic linkages are similar in the solid state and in water solution.[75] Thus, data from PDB should be useful in generating a second prior. The program GLYTORSION was used to search for the structural element α-D-Man*p*-(1→2)-α-D-Man*p*; 213 structures were found. The structures were analyzed with PDBCARE and two errors were found. As a third step, the ring torsions were checked, with GLYTORSION.[16, 76] A visual inspection of outliers was performed, and in uncertain cases the pdb-file was downloaded and the torsion angles measured. 13 errors were found during this inspection leaving 187 structures. A common mistake in the pdb-files is incorrectly assigned ligands; in this survey, 9 structures assigned as ligands were really *N*-glycans. Out of the final structures, 136 were *N*-glycans, 11 were *O*-glycans and 40 were ligands. These 187 fragments were used to generate the second prior, the DB-prior. The distribution is shown in *Figure 6.2*.

6.2.3 NMR spectroscopy

NMR spectroscopy was used to acquire experimental data to test how well the priors could predict the experimental observations. Proton-proton cross relaxation rates were obtained from 1D and 2D ^{1}H,^{1}H T-ROESY experiments and were interpreted as effective distances as discussed in section 2.4.2. The 1DLR experiment devised by Nishida *et al.*[36] was used to determine transglycosidic ^{1}H,^{13}C-coupling constants. Homonuclear ^{13}C,^{13}C-coupling constants were found in literature.[77, 78] Additional experimental data

was also used in the form of optical rotation.[79, 80] The experimental data can be found in Table 1 in paper III.

6.2.4 Data analysis

The two priors show all conformations in the same areas, $-90° < \phi_H < 80°$ and $-90° < \psi_H < 80°$. The mode of the distribution is slightly shifted between the two priors, and the MD-prior populates more negative ψ_H torsion angles than the DB-prior, see *Figure 6.2*. Expectation values were calculated for the two priors giving two posteriors, the MD-posterior and the DB-posterior. The agreement between either of the priors with the experimental data is not ideal. The distributions, shown in *Figure 6.4*, are clearly shifted towards the non-*exo*-anomeric conformation both for positive and negative ψ_H values. The population distributions significantly deviate from the priors as well as between each other. The analysis needed further improvement.

We decided to look closer at the Karplus equations used in the analysis. In empirical Karplus parameterizations reference molecules are used. There is an uncertainty and flexibility in the torsion angles of the reference molecules which results in a compressed Karplus curve.[81] For proton-proton coupling constants it is well established that electronegative substituents directly bonded to either of the central atoms in the coupling pathway decrease the magnitude of the coupling constant and induce an asymmetry in the Karplus curve. Altona *et al*. have developed well established relationships for proton-proton coupling constants.[82-84] For heteronuclear transglycosidic couplings the ring oxygen at the anomeric carbon is an inner substitutent for the ϕ related coupling pathways, but not for the ψ related pathways. Thus, it could be anticipated that different Karplus relationships should be used for the ϕ and ψ coupling constants. Zhao *et al.* have reported that internal electronegative substituents perturb $^3J_{COCC}$ Karplus curves by phase shifting them, and that the two types of interresidue C-O-C-C coupling pathways, *i.e.* ϕ and ψ, can not be treated using one generalized Karplus equation.[85] Bose *et al.* have also reported that if in-plane oxygens on either of the terminal carbons are present the observed coupling constant is increased by ~0.7 Hz.[68]

Considering these observations, we decided to reparameterize the $^3J_{COCH}$ and $^3J_{COCC}$ Karplus equations for ϕ and ψ, taking into account the effect of electronegative substituents. For three-bond couplings involving ^{13}C spins, two separate effects from electronegative substituents need to be considered, when the substituent is directly bonded to the ^{13}C (outer substituent), and when the substitutent is attached to either of the two central atoms (inner substituent). For outer substituents the effect is referred to as the *in-plane* effect. This effect has been described by Bose *et al.*[68] and is particularly important in carbohydrates. The in-plane effect is an increased coupling between C and Z for the fragment O-C-X-Y-Z when the O-C-X-Y dihedral

angle is 180°, *i.e.* the substituents are antiperiplanar. The in-plane effect can be either constant or variable. The variable in-plane effect is present when rotation around a sigma bond can position an oxygen atom in-plane to the torsion angle in question. For M2M the hydroxyl group attached to C2′ results in a constant in-plane (CIP) effect for $\phi_{C2'}$, and the ring oxygen O5′ results in a variable in-plane effect (VIP) for ψ when the $\phi_{O5'}$ torsion angle is close to antiperiplanar. For transglycosidic coupling constants, the inner substituent is the ring oxygen, O5′. This electronegative substituent decreases the coupling constants related to ϕ, and is referred to as the inner oxygen substituent (IOS). The atoms related to the different effects for M2M are highlighted in *Figure 6.1*.

The herein discussed perturbing effects were taken into account when reparameterizing new Karplus type equations for $^3J_{COCC}$ and $^3J_{COCH}$ for both ϕ and ψ, in total four new equations. The general form of the equations is:

$$^3J = A\cos^2(\theta+\delta) + B\cos(\theta+\delta) + C$$

where θ is the dihedral angle and δ is a potential phase shift, while A, B and C are empirical constants.

As a starting point for the $^3J_{COCC}$ relationship, the two-parameter equation proposed by Bose *et al.*[68], obtained for molecules lacking an in-plane effect and ignoring the inner oxygen substituent (IOS), was used. An average phase shift (Δ) of 12°[85, 86] was found when accounting for IOS and a decrease of A by 7% in the presence of IOS and an increase by 7% when IOS is absent. The constant in-plane effect, CIP, was accounted for by an addition of 0.6 Hz per in-plane oxygen atom. When a variable in-plane effect (VIP) is present, the effect is treated by a scaled distribution with the parameter κ. When κ=8 the in-plane effect is reduced to 50% of the full effect. The phase shift is dependent on the stereochemistry of the sugar residue with $\Delta = -12$ for α-D and $\Delta = +12$ for β-D hexoses. The proposed equations are:

$$^3J_{C,C}(\phi_{C2'}) = 3.72\cos^2(\phi_{C2'}+\Delta) - 0.08 + CIP$$

$$^3J_{C,C}(\psi_{C1'}) = 4.28\cos^2(\psi_{C1'}) - 0.11 + 0.6\exp(\kappa\cos(\phi_{O5'}-180))/\exp(\kappa) + CIP$$

For $^3J_{COCH}$ the corresponding equations proposed by Tvarovška *et al.*[87] were used as a starting point. To account for the IOS the C-coefficent is increased by 0.25 Hz in the absence of IOS and decreased by 0.25 Hz in the presence of IOS together with a 12° phase shift. The presence of a potential in-plane effect is treated in the same way as for the $^3J_{COCC}$ equations, giving the following relationships:

$$^{3}J_{C,H}(\phi_H) = 6.54\cos^2(\phi_H - \Delta) - 0.62\cos(\phi_H - \Delta) - 0.17$$

$$^{3}J_{C,H}(\psi_H) = 6.54\cos^2(\psi_H) - 0.62\cos(\psi_H) + 0.33 + 0.6\exp$$
$$(\kappa\cos(\phi_{O5'} - 180))/\exp(\kappa)$$

The corresponding Karplus curves for M2M are shown in *Figure 6.3* and the relationships are denoted JCX/SU09.

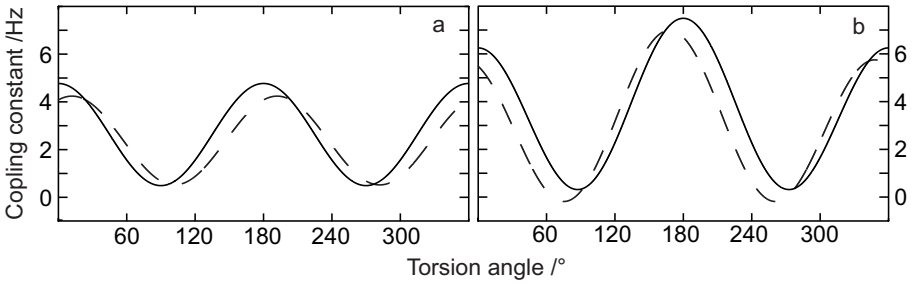

Figure 6.3. Karplus curves for JCX/SU09 for M2M, **a** shows $^{3}J_{C,C}$ for $\phi_{C2'}$ (dashed line) and $\psi_{C1'}$ (solid line) and **b** shows $^{3}J_{C,H}$ for ψ_H (solid line) and ϕ_H (dashed line).

New posteriors relative the MD- and DB-priors were calculated with the maximum entropy formalism using the new Karplus relationships. When comparing the priors and the posteriors, see *Figure 6.4*. The mode for the MD-posteriors is shifted and becomes more similar to the DB-posterior when the new JCX/SU09 equations are used. The population having $\psi_H >$ 45° is also decreased in the new posterior; this conformation is only populated by three structures in the database survey. The population having large ψ_H values seems to be overestimated by the force-field. Also, the population of the third quadrant increased in the new posteriors, becoming intermediate between the two priors. The biggest difference using the new JCX/SU09 Karplus relationships is the absence of the large population in the fourth quadrant. The two new posteriors have very similar populations in the four quadrants. The difference between the priors and the posteriors when using the JCX/SU09 relations is small.

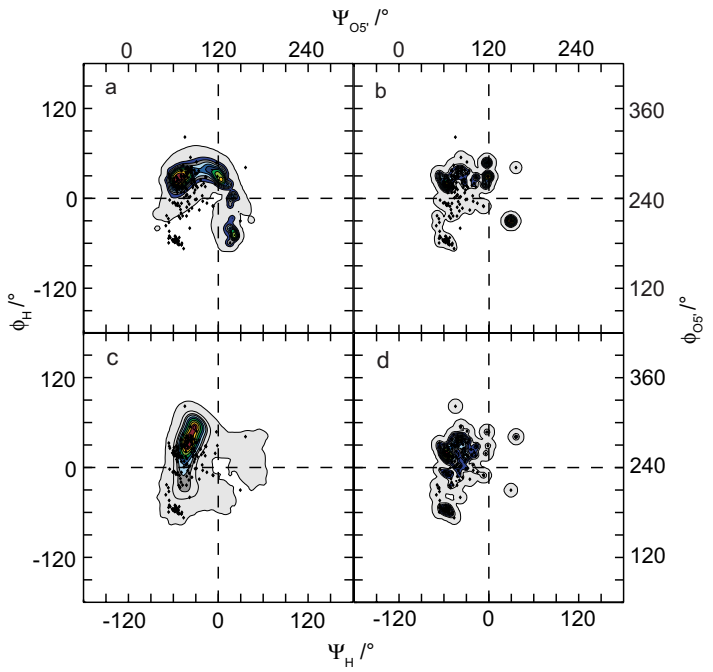

Figure 6.4. Posteriors obtained from the ME-analysis of the spectroscopic data using the prior from the MD simulation, (a) and (c) or the DB prior, (b) and (d). For (a) and (b) Karplus relations from ref Cloran *et al.*[25] were used and for (c) and (d) the JCX/SU09 relations presented herein were used. The outermost curve covers up to 90% of the population, increments are given in 10% intervals.

6.3 Conclusions

A general approach to obtain conformation population distributions of flexible molecules has been described. Background information from MD-simulations and X-ray crystallography data from databases were used to generate priors as starting points for further analysis. NMR spectroscopy was used to obtain experimental data in solution, namely proton-proton distances and homo- and heteronuclear coupling constants related to the glycosidic torsion angles. The maximum entropy approach was used to get converged population distributions from the priors. Four new Karplus relations for the ϕ and ψ torsion angles were formulated. The new Karplus equations give very small differences between the priors and posteriors and lead to significantly improved descriptions of the conformational space.

This new methodology gave an excellent description of the disaccharide M2M studied herein. M2M exists in a conformational equilibrium where the *exo*-anomeric effect is the major influence on the ϕ torsion angle. The ψ

torsion angle has two major states, one with $\psi_H > 0$ and one with $\psi_H < 0$, the states being populated to ~3:1.

The deviations seen between the MD simulation and the MD posterior is a result of an overestimation of large ψ_H values by the force field. These findings may facilitate further developments of this force field. The method developed can be used for more complex molecules with a larger number of degrees of freedom, such as larger oligosaccharides or for biomolecules in general.

7 Structural analysis of the exopolysaccharide produced by *Streptococcus thermophilus* ST1 solely by NMR spectroscopy (paper IV)

7.1 Introduction

Streptococcus thermophilus is a major dairy starter used in yoghurt and cheese production.[88] The texture of yoghurt is strongly dependent on the physical and structural properties of the exopolysaccharide (EPS), such as type, sugar composition and degree of branching.[89] In the present study, the *S. thermophilus* strain ST1 was found to produce a viscous EPS when grown in skimmed milk.

Several different EPSs produced by *S. thermophilus* strains have been studied previously and the first strain was characterized in 1990.[90] The repeating units of the structure of *S. thermophilus* EPS vary considerably and range from tetrasaccharides[91] to heptasaccharides[92]. The EPSs of *S. thermophilus* are neutral or polyanionic heteromers primarily composed of D-galactose, D-glucose, and L-rhamnose, but also N-acetyl-D-galactosamine, acetylated D-galactose and D-ribose. Moreover, the molecular masses of these polymers differ and many of them are highly viscous. Nordmark *et al.*[93] have explained the high viscosity of a branched pentasaccharide repeating unit of D-galactose and D-glucose by the side-chain composition.

To understand the viscosity properties of the EPS produced by *S. thermophilus* ST1 we wanted to elucidate the structure of the repeating unit of the polysaccharide.

7.2 Structure elucidation

The EPS produced by *Streptococcus thermophilus* ST1 was isolated from skimmed milk. Size exclusion chromatography confirmed that the sample was uniform and had a molecular weight of >20 kDa. The proton NMR spectrum of the polysaccharide showed six resonances in the anomeric region, between 4.5 and 5.1 ppm, see *Figure 7.1*. The rest of the resonances

are all situated within less than 1 ppm in the crowded ring region of the spectrum.

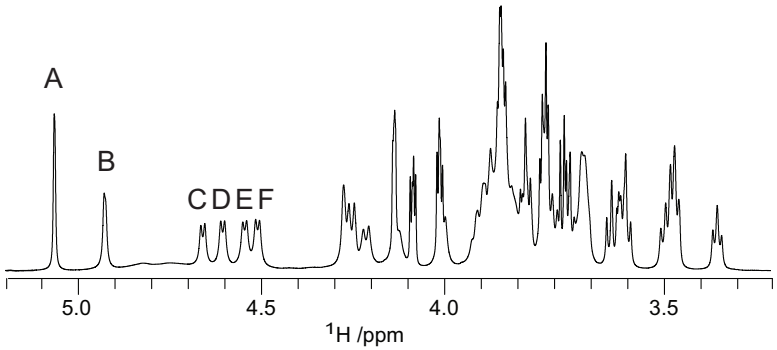

Figure 7.1. ^{1}H NMR spectrum of the EPS of ST1 at 700 MHz with presaturation. Six signals can be seen in the anomeric region, the corresponding residues are denoted **A**-**F**.

Next, a ^{13}C spectrum was collected in parallel with a ^{1}H,^{1}H TOCSY spectrum, see *Figure 7.2*. This is possible when using a spectrometer equipped with parallel receivers so that the ^{13}C spectrum can be collected during the spin-lock of the TOCSY experiment[94]. Six spin systems could be identified, *i.e.* six monosaccharide units are present in the repeating unit, confirming what was seen in the ^{1}H NMR spectrum. The spin-systems were denoted **A**-**F** starting from the anomeric proton with the highest chemical shift.

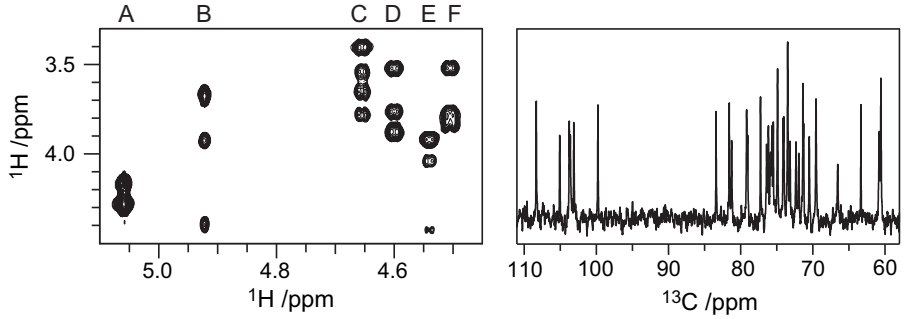

Figure 7.2. A TOCSY spectrum with a 120 ms long spin-lock (left); during the spin lock a separate ^{13}C experiment was acquired with the help of dual receivers (right).

An HSQC experiment showed six cross-peaks in the anomeric region as well as six pairs of cross-peaks in the methylene region, indicating that the six monosaccharide units were hexoses. The ^{1}H and ^{13}C chemical shifts are indicative of the sugar composition of the polysaccharide. The absolute configuration, on the other hand, can not be determined directly from the underivatized polysaccharide. The identities of the constituent sugar components and their absolute configurations were determined by NMR spectroscopy as devised by York *et al.*[18] The EPS of ST1 was hydrolysed and treated with SMB (per-*O*-*(S)*-2-Methylbutyric anhydride) to give single di-

astereomers of the monosaccharide units. These were compared to reference compounds prepared in the same manner, see *Figure 7.3*. Integration of ^{1}H resonances from D-glucose and D-galactose between 6.0 and 6.5 ppm showed a relative ratio of 3.7:2. Thus, the EPS of ST1 contains two different monosaccharide units, D-glucose and D-galactose present in a relative ratio of 2:1. No chromatographic methods and only one wet chemical procedure was needed to determine both the identity and the absolute configuration of the constituent sugars of the polysaccharide.

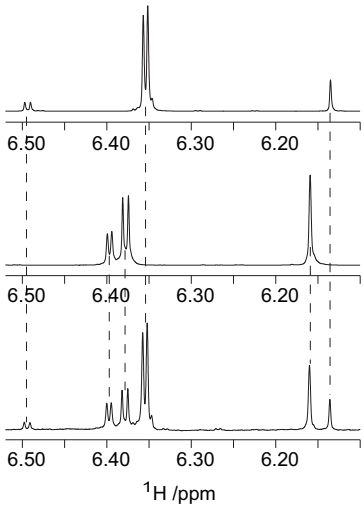

Figure 7.3. Component analysis with ^{1}H NMR spectroscopy of the EPS from ST1, (top) D-glucose-SMB, (middle) D-galactose-SMB and (bottom) EPS-SMB hydrolysate.

The four anomeric resonances, **C**-**F**, all have large $^{3}J_{H1,H2}$ coupling constants ($^{3}J_{H1,H2}$ = 7.5 Hz). In the case of D-gluco- and galactopyranosides, this means that they have the β-configuration. From chemical shifts and coupling constant patterns, residues **C**, **D** and **F** are assigned to be β-D-Glc*p,* whereas residue **E** is a β-D-Gal*p*. The other two anomeric resonances, **A** and **B**, do not show resolved coupling constants, but the half-widths indicate that the coupling constants are much smaller. Furthermore, the $^{1}J_{C1,H1}$ coupling constants extracted from a non-decoupled HSQC spectrum confirmed that residues **C-F** are β-linked and that residue **B** ($^{1}J_{C1,H1}$ = 172 Hz) is α-linked. Again, chemical shifts reveal that **B** corresponds to a β-D-Glc*p*. From ^{13}C chemical shifts of C1 and C4 as well as an HMBC correlation between H1 and C4 **A** was determined to be a furanoside. The $^{1}J_{C1,H1}$ coupling constant for **A** does not distinguish between the α and the β form but the unresolved $^{3}J_{H1,H2}$ coupling constant is small indicating a β-linked furanoside. To the best of our knowledge, β-D-Glc*f* has only been reported once,[95] whereas β-linked D-galactose in a furanoside ring form, *i.e.* β-D-Gal*f* is present in many bacterial polysaccharides. The chemical shifts of residue **A** was compared to

corresponding chemical shifts of the methyl glycosides of β-D-Glc*f* and β-D-Gal*f*.[96] The deviation for C1 and C6 is twice as large for glucose (1.2 ppm) as for galactose (0.6 ppm); therefore, residue **A** was assigned to be a β-D-Gal*f* residue.

The complete assignment of all ^{1}H and ^{13}C chemical shifts can be found in Table 1 in paper III. A number of 2D-NMR experiments were used to assign all the resonances in residues **A**-**F**. A series of 2D TOCSY experiments with mixing times ranging from 10-120 ms gave information on the different spin-systems. An H2BC experiment, showing only two-bond ^{1}H-^{13}C correlations facilitated the analysis of the six spin-systems.

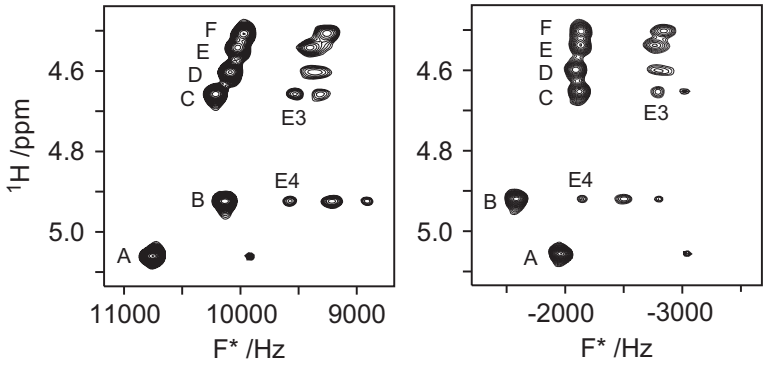

Figure 7.4. NOESY-HSQC TILT NMR experiment with α=+15, left and α=-15, right.

For the assignment of the galactopyranose, 2D NOESY-HSQC-TILT[20, 21] experiments were used to overcome the problems with the small $^{3}J_{H4,H5}$ coupling constant ($^{3}J_{H4,H5}$ < 1Hz) and resonance overlap, see *Figure 7.4*. The TILT experiment uses projections of mixed ^{1}H and ^{13}C frequencies onto a tilted plane (F*). From two experiments with two different tilt angles, in this case ±15°, the chemical shifts can be extracted without the collection of a full 3D-experiment but with more resolved peaks than in a 2D experiment. The TILT experiment is one order of magnitude faster than a 3D NOESY-HSQC experiment.

Table 7.1. Inter-residue correlations observed in the $^{1}H,^{13}C$ HMBC and $^{1}H,^{1}H$ NOESY spectra with 55 ms mixing time of the EPS from ST1.

Sugar residue	Residue	Anomeric atom	Residue	HMBC	NOE
β-D-Gal*f*-(1→	**A**	H1	**D**	C6	H6a
α-D-Glc*p*-(1→	**B**	H1	**E**	C4	H4, H6a (w), H6b (w)
	B	C1	**E**	H4	
→6)-β-D-Glc*p*-(1→	**C**	H1	**E**	C3	H3
	C	C1	**E**	H3	
→4,6)-β-D-Glc*p*-(1→	**D**	H1	**C**	C6	H6a
3,4)-β-D-Gal*p*-(1→	**E**	H1	**F**	C4	H4, H6a (w), H6b (w)
	E	C1	**F**	H4	
→4)-β-D-Glc*p*-(1→	**F**	H1	**D**	C4	H4
	F	C1	**D**	H4	

(w) = weak NOE.

As discussed in section 2.2, glycosylation shifts give valuable information on the substitution pattern of the different residues in a polysaccharide. All the glycosylation shifts for the EPS of ST1 can be found in Table 1 in paper III. The anomeric carbon resonances are shifted by 6.2–8.5 ppm and the substituted carbons show glycosylation shifts of 4.8–6.8 ppm. Residue **C** is 6-substituted, residue **F** is substituted in position 4. Residues **D** and **E** are disubstituted with 4,6- and 3,4-substitution, respectively. Thus, the structure has to be branched. Residues **A** and **B**, which only show glycosylation shifts on the anomeric carbons, must be terminal groups.

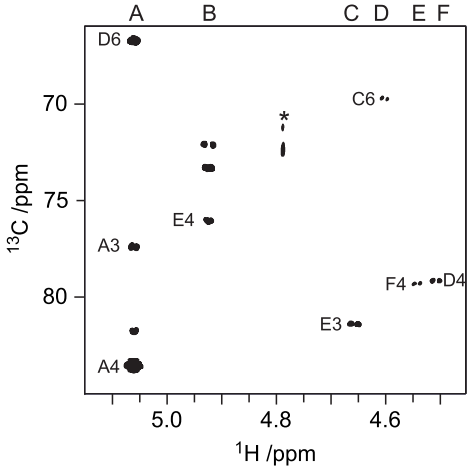

Figure 7.5. Part of the HMBC spectrum of the EPS from ST1 showing interresidue $^{3}J_{C,H}$ correlations, artifacts from the HDO resonance is marked by an asterisk.

The substitution patterns are summarized in *Table 7.1*, and part of the HMBC spectrum is shown in *Figure 7.5*. The sequence of the six residues was determined by HMBC and NOESY experiments. The transglycosidic correlations found are presented in *Table 7.1*. The repeating unit structure is shown in *Figure 7.6* .

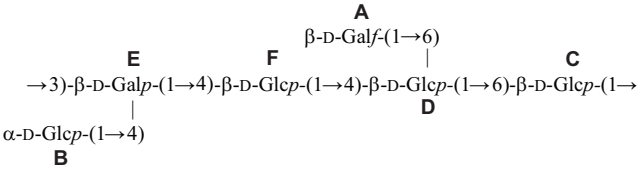

Figure 7.6. Structure of the EPS from ST1.

As mentioned above, the EPS from ST1 yielded a highly viscous sample. The molecular weight of the polysaccharide was investigated with translational diffusion measurements. First, the sample was diluted until no change in the diffusion constant could be detected, 0.6 mg/ml. The diffusion constant was determined by NMR spectroscopy[97] to be $D_t = 3.50 \times 10^{-11}$ m^2s^{-1}. The molecular weight was calculated according to Viel *et al.*[98] to be 61.9 kDa, corresponding to 64 repeating units with six hexoses per unit. The diffusion constant measured by NMR spectroscopy was compared to measurements by dynamic light scattering, DLS, giving a corresponding molecular weight of 51.9 kDa.

7.3 Conclusions

It was possible to determine the primary structure of the EPS from ST1 solely by NMR spectroscopy. The sugar composition was determined from ^{1}H and ^{13}C chemical shifts and coupling constant patterns and was confirmed by the absolute configuration determined by ^{1}H NMR spectroscopy. To elucidate the primary structure ^{1}H and ^{13}C NMR spectroscopy, including 2D ^{1}H,^{1}H TOCSY, ^{1}H,^{1}H NOESY, ^{1}H,^{13}C HSQC, ^{1}H,^{13}C H2BC and ^{1}H,^{13}C HMBC experiments were used. To resolve ambiguities due to spectral overlap in the 2D NOESY spectra, tilted projections of a three-dimensional ^{1}H,^{1}H NOESY-^{1}H,^{13}C HSQC spectrum were recorded. By the use of tilted projections where the ^{13}C and ^{1}H evolutions are linked together, the need to record a full three-dimensional spectrum was avoided.

The high viscosity of the EPS may be explained by the branching pattern present in the repeating unit. It was possible to get high resolution and narrow peaks in spite of the high molecular weight of the polysaccharide; this is due to internal motions in the structure.

Knowledge of the primary EPS structure will now facilitate further investigations relating polysaccharide structure and dynamics to rheological properties.

8 The dynamics of GATG glycodendrimers by NMR diffusion and quantitative ^{13}C relaxation (paper V)

8.1 Introduction

Dendrimers are branched synthetic macromolecules with a globular shape. They are synthesized by iterative controlled steps, are monodisperse and may exhibit different environments at their core and at the periphery. These unique properties have made them very useful in many different areas, such as host-guest chemistry, catalysis, materials science, drug and gene delivery and *in vivo* imaging.[8, 99-101] To develop new applications for dendrimers, knowledge about size, shape and dynamics is crucial.

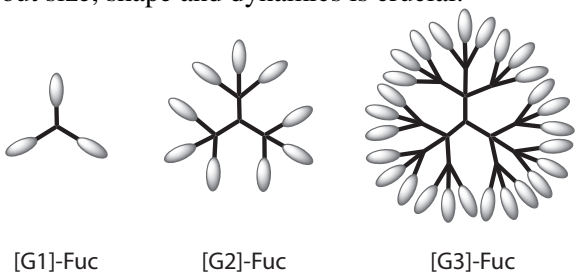

Figure 8.1. Schematic picture of the three generations of glycodendrimers decorated with fucose moieties shown as gray ovals.

Gallic acid-triethylene glycol (GATG) dendrimers are a dendrimeric family which potentially can be used in biomedical applications, including drug delivery and multivalent carbohydrate recognition.[102, 103] They are easily functionalized and the spacer arms are expected to give them considerable flexibility. Glycans that participate in multivalent cell-cell interactions and cell migration processes often have L-fucose as their terminal group.[104] For that reason, we have investigated three generations of fucose decorated GATG dendrimers (G1-[Fuc], G2-[Fuc] and G3-[Fuc]). The dendrimers were synthesized with click chemistry as described by Fernandez-Megia *et al.*[105] A schematic representation of the dendrimers can be seen in *Figure 8.1*, for a detailed description see Figure S1 in supporting information of paper V.

Previously studies of size, conformation and dynamics of dendrimers have been made using small angle neutron scattering (SANS), small angle X-ray scattering (SAXS) and NMR spectroscopy along with computer simulations.[106, 107] To the best of our knowledge, a study of the internal dynamics of PAMAM (poly(amido amine)) dendrimers is the only quantitative study of dendrimer dynamics made with NMR spectroscopy.[108-110] For GATG dendrimers Fernandez-Megia *et al.* have reported a qualitative analysis by ^{1}H NMR spectroscopy of the internal dynamics in $CDCl_3$.[111] To further increase the understanding of the dynamics of the GATG glycodendrimers and to aid ongoing bioapplications, quantitative investigations in aqueous solution is valuable. Thus, we wanted to quantitatively investigate these dendrimers in aqueous solution by NMR spectroscopy in combination with the Lipari-Szabo model-free approach.[40, 112]

8.2 Results and discussion

8.2.1 Diffusion measurements

To make quantitative diffusion measurements the sample should be under extremely dilute conditions. We recorded ^{1}H PFG NMR experiments at three different concentrations (1, 0.3 and 0.1 g/L) of G1-[Fuc], G2-[Fuc] and G3-[Fuc]; the diffusion coefficient D_0 remained unchanged for concentrations $\leq$ 0.3 g/L. Also, the spin-echo decays were identical for varying diffusion times, Δ (100 and 300 ms). Thus, the dendrimers are under extremely dilute conditions and $D_t \sim D_0$, meaning that the diffusion is entirely dependent on size. The diffusion coefficients were measured using a LED-BPSTE pulse sequence.[113] The Stejskal-Tanner equations[46] were used to determine the diffusion coefficeients, as described in section 2.5. The Stejskal-Tanner plots are shown in *Figure 8.2* and the diffusion coefficients are listed in *Table 8.1*.

Table 8.1. Diffusion coefficents (D_0) of the three generations at a concentration of 0.3 g/L. The hydrodynamic radius (R_h) and the rotational correlation times (τ_R) calculated from the Stokes-Einstein and Debye-Stokes equations.

	[G1]-Fuc	**[G2]-Fuc**	**[G3]-Fuc**
M_w /Da	1289	4295	13337
D_0 /$m^2s^{-1}\times10^{-10}$	3.12 (0.13)[a]	2.12 (0.05)	1.41 (0.02)
R_h /nm	0.72 (0.03)	1.10 (0.02)	1.60 (0.02)
τ_R /ns	0.43 (0.06)	1.30 (0.10)	4.50 (0.20)

[a]Standard deviation is given in parenthesis.

Qualitative information about the density distribution within macromolecules can be gained from diffusion measurements. D_0 is related to the mo-

lecular weight (M_w) through a scaling exponent (α).[114] If the density distribution of the macromolecule is independent of the molecular weight, a scaling exponent of 0.33 is predicted. For macromolecules with an increasing density distribution with M_w, α is lower than 0.33 and for distributions which decrease with M_w, α is higher than 0.33. For the three [Gn]-Fuc dendrimers, the logarithm of the diffusion values were plotted against the logarithm of the molecular weights giving $\alpha = 0.34$, see *Figure 8.2*. This value indicates a spherical shape and a nearly homogeneous distribution of the density.

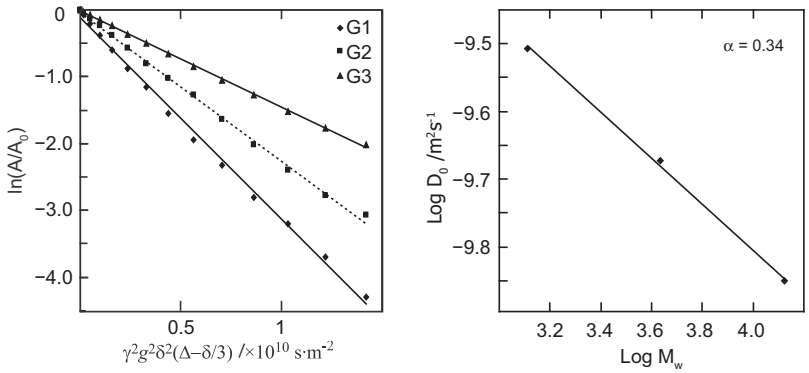

Figure 8.2. Stejskal-Tanner Plot for [G1]-Fuc (dimonds), [G2]-Fuc (squares), and [G3]-Fuc (triangles) at 0.3 g/L (left) and logarithmic plot of D_0 *vs.* M_w for [Gn]-Fuc (right), y = −0.34x −8.45.

The spherical shape and globular character of the [Gn]-Fuc dendrimers make it possible to use the Stokes-Einstein and Debye-Stokes relationships (see section 2.5) to estimate the hydrodynamic radii (R_h) and the rotational (global) correlation times (τ_R), listed in *Table 8.1*. From the diffusion measurements, information about the shape (spherical), size (R_h) and overall dynamics (τ_R) was obtained.

8.2.2 ^{13}C-relaxation studies

The diffusion measurements of the [Gn]-Fuc dendrimers gave information about the dynamical behavior at a time scale of nanoseconds. The homogenous density distribution found indicates flexibility and a dynamic behavior. To be able to further investigate the dynamics of the [Gn]-Fuc dendrimers, we used ^{13}C NMR relaxation. Relaxation of protonated carbons is much easier to quantify than ^{1}H relaxation. The relaxation is dominated by dipole-dipole interactions with the directly attached protons. The chemical shift anisotropy (CSA) is small, but not necessarily negligible.

First, an assignment of the ring fucosyl carbons and three of the core carbons was made with 1D ^{13}C DEPT-135, 2D ^{1}H,^{13}C HSQC and ^{1}H,^{13}C HMBC experiments.

The carbon-13 relaxation data was collected for the fucosyl ring carbons and for the three assigned core carbons at three different magnetic fields, 11.7, 14.1 and 16.4 T. For [G1]-Fuc, only two of the core carbons are present in the structure. Three different relaxation parameters were measured, namely, ^{13}C T_1, ^{13}C T_2 and heteronuclear $^{1}H,^{13}C$ NOE. Each experiment was repeated 1-3 times and the average value was used. When analysing the collected data it was found that carbons 1 and 4 on the one hand and carbons 2, 3 and 5 on the other hand exhibited very similar relaxation behavior. Hence, we decided to treat them in groups and use the average. The results are presented in *Table 8.2*. An explanation of this behavior is that the peripheral fucosyl groups have a local anisotropic movement.

Table 8.2. Relaxation parameters for carbons C1 and C4 on the one hand and C2, C3 and C5 on the other hand in [G1]-Fuc to [G3]-Fuc.

B_0 /T		**[G1]-Fuc**		**[G2]-Fuc**		**[G3]-Fuc**	
		C1, 4	C2, 3, 5	C1, 4	C2, 3, 5	C1, 4	C2, 3, 5
11.7	T_1/ms	545	483	466	408	432	378
	T_2/ms	n.d.	n.d.	n.d.	n.d.	300	258
	$1+\eta$	2.52	2.43	2.30	2.21	2.19	2.08
14.1	T_1/ms	596	539	525	458	492	428
	T_2/ms	473	424	382	339	329	270
	$1+\eta$	2.35	2.32	2.18	2.12	2.04	1.97
16.4	T_1/ms	614	544	536	476	520	470
	T_2/ms	505	438	408	369	328	281
	$1+\eta$	2.36	2.30	2.10	1.95	2.01	1.93

n.d. not determined

T_1 was determined by inversion recovery experiments with eight relaxation delays ranging from 5 ms to 2 s; a recovery delay time of $>5\times T_1$ was used. As can be seen in *Table 8.2*, T_1 increases with higher magnetic field strength and decreases with each generation. A CPMG pulse sequence using 8 relaxation delays between 20 ms and 1 s was used to measure T_2. T_2 values follow the same pattern as T_1, higher values with higher magnetic field strength and shorter values with increasing generation. For all generations, T_1 is longer than T_2. The NOE factors ($1+\eta$) were determined from the ratio of two dynamic NOE experiments, one with a short relaxation delay, 1 ms, and one with a long relaxation delay, 2 s. In contrast to T_1 and T_2, the NOE factors decrease with increasing magnetic field strength, but follow the same trend as T_1 and T_2 when going to a higher generation. The fact that all three parameters become shorter when increasing the generation suggests a slowdown of the motions responsible for the relaxation process. Since T_1 is

longer than T_2 for all three [Gn]-Fuc generations, they are outside the extreme narrowing region and must have relatively long correlation times.

Table 8.3. Relaxation parameters for carbons ***a***, ***b***, and ***c*** in [G1]-Fuc to [G3]-Fuc.[a]

B_0 (T)		**[G1]-Fuc**		**[G2]-Fuc**			**[G3]-Fuc**		
		Ca	Cb	Ca	Cb	Cc	Ca	Cb	Cc
11.7	T_1/ms	588	586	502	478	354	535	529	440[b]
	T_2/ms						240	202	46[b]
	$1+\eta$	2.42	2.38	2.20	2.09	2.03	2.04	1.91	1.50[b]
14.1	T_1/ms	646	588	573	521	426	488	500	368[b]
	T_2/ms	404	536	382	366	n.d.	272	299	n.d.
	$1+\eta$	2.51	2.43	2.17	2.05	1.45	2.06	1.86	1.65[b]
16.4	T_1/ms	651	656	572	546	400	570	550	280[b]
	T_2/ms	560	364	418	364	258	360	240	164[b]
	$1+\eta$	2.29	2.23	2.03	1.91	1.55	1.94	1.84	1.49[b]

[a]Relaxation times are reported as NT_1 and NT_2 (N = number of H atoms directly bound to the carbon atom). [b]As shown in Figure S1, for [G3]-Fuc, carbon ***c*** represents two different carbons of internal sub-shells not resolved by ^{13}C NMR.

The difference in relaxation between the core and the periphery was also investigated and the results are summarized in *Table 8.3*. Previous NMR relaxation studies of dendrimers have shown that there is less mobility in the core than at the periphery. This has also been predicted by theoretical studies.[115] The internal carbons (carbons **a**, **b** and **c**) investigated were all CH_2 groups and may exhibit cross relaxation effects, but this effect was considered to be small according to the monoexponential behavior of their respective T_1 and T_2. Furthermore, the analysis is made more difficult by the fact that the resonance for carbon **c**, corresponds to two different sub-shells for [G3]-Fuc. In spite of these problems some trends can be seen, [G2]-Fuc and [G3]-Fuc shows lower T_1, T_2 and Het-NOE values for carbon **c** than for carbons **a** and **b** and lower than for C1-C5 in the fucose ring. When going to a higher generation the relaxation parameters decrease for the three core carbons. This data indicates that the mobility at the core is reduced on increasing the generation, in agreement with previous studies of azide-terminated GATG[111] and PAMAM dendrimers[109, 110], as discussed above.

8.2.3 Model-free fittings

A quantitative analysis of the relaxation data was made for the carbons in the fucosyl group. The relaxation rates were fitted to model-free parameters using R_1, R_2 and Het-NOE. The Lipari-Szabo model-free approach was used with the Modelfree software developed by the Palmer group.[41] The motional behavior of the fucosyl groups was best described by model 2. In model 2,

the global correlation time (τ_m) is fitted as well as the general order parameter (S^2) and the internal correlation time (τ_e). The parameters obtained from model 2 are listed in *Table 8.4*. The differences in τ_e and S^2 for C1 and C4 compared to C2, C3 and C5 agree with the relaxation data presented in *Table 8.2*.

Table 8.4. Modelfree data for the [Gn]-Fuc dendrimers, standard deviations are shown in parentheses.

		[G1]-Fuc	**[G2]-Fuc**	**[G3]-Fuc**
χ^2 (Total/95%)		3.4/19.6	8.5/19.8	6.28/23.44
τ_m/ns		1.08	1.00	1.36
τ_e/ps	C1, 4	91 (6)	95 (8)	100 (9)
τ_e/ps	C2, 3, 5	107 (9)	114 (11)	125 (13)
S^2	C1, 4	0.13 (0.02)	0.23 (0.02)	0.27 (0.02)
S^2	C2, 3, 5	0.15 (0.02)	0.27 (0.03)	0.34 (0.02)

The τ_m values represent the global correlation time, and are typically associated with a globular rotation of globular proteins. The overall rotation is expected to be reduced with higher dendrimer generation, this is not the case for [Gn]-Fuc (τ_m = 1.08 ns for G1, 1.00 ns for G2 and 1.36 ns for G3). The τ_m values are also, in contrast with the τ_R values, obtained from the PFG diffusion measurements, which were τ_R = 0.43 ns for G1, 1.30 ns for G2 and 4.50 ns for G3. Rather than the overall motion we identify τ_m as a slow internal motion independent of generation. This kind of pulsating motion has previously been reported for polysaccharides.[116] The higher value of τ_m compared to τ_R for G1 could also be explained by the much higher concentration used in the relaxation measurements (20 g/L *vs.* 0.3 g/L) which could lead to more intramolecular interactions.

A recent theoretical work by Markelov *et al.*[115] proposed that the dendrimer segmental orientational mobility is governed by three main relaxation processes: (i) the rotation of the dendrimer as a whole, (ii) the rotation of the dendrimer's branch originated from a given segment, and (iii) the local reorientation of the segment, an internal correlation time. The rotation of the dendrimer corresponds to the rotational correlation time; the rotation of the branch depends on the distance between this segment and the periphery of the dendrimer and is a pulsating motion. It is also concluded that the rotational correlation times have a small contribution on the auto-correlation of the peripheral groups, in our case the fucosyl units. This is in accordance with what we have seen from the results by the Modelfree fittings for the [Gn]-Fuc dendrimers. Thus, τ_m is identified as the pulsating correlation time related to the rotation of the dendrimer branch and τ_e is identified as the internal correlation time related to the local reorientation of the C-H vector in

the sugar ring. S^2 reflects the flexibility of the molecules and gives information on the importance of the local reorientation and the pulsations in the relaxation process, where the local reorientation is the more important motion. The overall motion of the dendrimers may have an influence on the S^2 values, which are increasing with each generation and on the small increase in τ_m that was observed.

8.3 Conclusions

To the best of our knowledge, this study is the first quantitative study performed on dendrimers with the Liari-Szabo model-free approach using carbon-13 relaxation data. A previous study using proton NMR relaxation parameters for PPI dendrimers, at only one magnetic field has been reported[117]. The study was, however, only semi-quantitative.

Three different correlation times were identified for the dendrimers. First, the global correlation time, τ_R, or the rotation of the dendrimer as a whole, was determined by PFG NMR diffusion measurements and increases with the size of the dendrimer. Secondly, the local reorientation of the C-H vector, τ_e, which is independent on the generation of the dendrimer. And lastly, τ_m, the rotation, or pulsation of a dendrimer branch. The two latter correlation times were determined by model-free fittings of ^{13}C relaxation data acquired at three different magnetic field strengths.

Dendrimer dynamics can successfully be studied quantitatively with the model-free approach from ^{13}C NMR relaxation data. An improved description of the motions involved in the relaxation of dendrimers could be obtained by the implementation of alternative correlation (and spectral density) functions weighting the influence of the overall and local motions, such as the one proposed by Markelov *et al.*[115]

9 Conclusions

Carbohydrate-containing biomolecules play many important roles in nature. In this thesis several glycoconjugates have been investigated with different techniques.

In paper I, the ring conformations of two chemically synthesized carbaiduronic acids were successfully investigated with NMR spectroscopy. The results showed that $^4C_1$ is the predominant conformation. It would be interesting to extend this study to include sulfated carbaiduronic acids and carbaiduronic acids as parts of larger oligosaccharide structures to investigate whether the ring conformation is the same in those cases.

In paper II NMR spectroscopy was used in combination with molecular dynamics simulations to investigate the conformation around the glycosidic linkage of two isotopically labelled 1→6 linked disaccharides related to an oligosaccharide epitope expressed on malignant tumor cells. The combination of NMR spectroscopy, MD simulations, spin simulations and crystal structure data proved powerful.

In paper III, the conformational space of α-D-Man*p*-(1→2)-α-D-Man*p*-OMe was investigated by applying the maximum entropy analysis using different priors as background information. Four new Karplus relationships denoted JCX/SU09 are also presented. The methodology presented in the paper could be applied to different flexible molecules.

The hexasaccharide structure of the EPS produced by *S. thermophilus* ST1 was elucidated solely by NMR spectroscopy in paper IV. The NMR investigation included component analysis, and absolute configuration and molecular weight investigations. A number of different 1D and 2D techniques were used.

The dynamics of three generations of GATG glycodendrimers was investigated with NMR spectroscopy in paper V. The correlation times describing the motions of the dendrimers were found by NMR translational diffusion and by a quantitative analysis was performed with the Lipari-Szabo model-free approach of ^{13}C-relaxation data.

Acknowledgments

Många har hjälpt mig på olika sätt med mitt avhandlingsarbete de senaste åren, jag vill tacka:

Göran Widmalm för att du antog mig som doktorand i din grupp, för intressanta projekt, tålamod och mycket tid!

Jan-Erling Bäckvall för visat intresse.

Ian, Jerk, Jens och *Robert* för att ni hjälpt till att förbättra avhandlingen både innehållsmässigt och språkligt.

Past and present members of the *GW group*: *Mona* for being a great friend, *Jerk* for your enthusiasm when it comes to chemistry, *Christoffer* for organizing stuff, *Robert* for Lekstugan!, *Carolina* for making the group a bit more international, *Olle* for being such a happy guy, *Thibault* for nice lunch company this summer, *Magnus* for all the computer support, *Hannaj* for much fun at and outside work, *Jens* for NMR support, *Mattias* for good collaboration and lots of fun, *Ulrika* for being such a wonderful person, *Tara* for good times in the lab, *Jennie* for all the help my first year as a PhD student, *Ramon* for great collaboration on the dendrimer project. My diploma workers: *Johanna, Lilly, Florian,* and *Ana.*

All my co workers on different projects, especially: *Jennie, Ulrika, Hannaj, Mattias, Ramon, Jerk* and *Robert*.

Torbjörna Astlind för all overdelig hjälp med spektrometrarna.

Alla i *TA personalen* för hjälp med allt mellan himmel och jord.

Ulf Ellervik för allt du lärde mig om kolhydratskemi och för att du väckte mitt intresse för forskning!

För mycket trevligt rese- och konferenssällskap:

Mona, Annika, och *Lisa* för en fantastisk resa till Washington DC.
Mona, Jens, Ulrika och *biofysikfolket* för en trevlig konferens i Göteborg.

Jens för konferensen i Santa Fe.

Jens, Johan, Ricky och många fler för kul i Budapest.

Hannaj, Ulrika, Tara, Johan, Clinton, Ricky och *Jens* för resan till Lübeck.

Alla doktorander som var med i Kalmar, speciellt *Hannaj, Johan* och *Jens.*

AstraZenecas resestipendium till minne av Nils Löfgren, K & A Wallenbergs resestipendium, kemist samfundet, SMASH och EUROMAR för bidrag till konferensresor.

SNC, for a great NMR facility.

Anna, *Marcin* och *Mikaela* för många trevliga luncher!

Jane and *Jazzy, Rasa* and *Mia* for making the year in York such a good experience!

All my friends and family from Minnesota, especially: *Stephanie*, *Amanda*, *Debbie*, *Dave*, *Todd* and *Amy*. I hope that you can come visit us in Sweden one day!

Kursarna från Lund, speciellt *AnnaE*, *Åsa*, *AnnaL* och *Marcin*.

Alla vänner utanför avdelningen speciellt *Jenny, Cissi, Mirja* och *Katta* för massa kul i Stockholm.

Alla tjejerna från Sundsvall, *Malin, Jessica, Maria, Anna* och *Lisa* för att ni alltid finns där och för att allt är som det alltid varit!

Min familj, *mamma*, *pappa*, *Petter* och *Joel* med familjer!

Jens för allt!

Ingrid för att du sov middag under hösten så att jag kunde skriva den här avhandlingen!

References

1. Lindhorst, T. K. In *Essential of carbohydrate chemistry and biochemistry;* Wiley-VCH: Weinheim; Chichester, 2007.
2. Varki, A. In *Essentials of glycobiology;* Cold Spring Harbor Laboratory Press: New York, 1999.
3. Sutherland, I. W. *Trends Biochem. Sci.* **1979**, *4*, 55-59.
4. Rehm, B. H. A. **2010**, *8*, 592.
5. Lepenies, B.; Yin, J.; Seeberger, P. H. *Curr. Opin. Chem. Biol.* **2010**, *14*, 404-411.
6. Cumpstey, I. *Carbohydr. Res.* **2009**, *344*, 2285-2310.
7. Fernandez-Megia, E.; Correa, J.; RodrÃguez-Meizoso, I.; Riguera, R. **2006**, *39*, 2120.
8. Lee, C. C.; MacKay, J. A.; Frechet, J. M. J.; Szoka, F. C. *Nat. Biotechnol.* **2005**, *23*, 1517-1526.
9. Kamerling, J. P.; Boons, G. In *Comprehensive glycoscience;* Elsevier: Amsterdam; Boston, 2007.
10. Boons, G. In *Carbohydrate chemistry;* Blackie Academic & Professional: London, 1998.
11. Stoddart, J. F. In *Stereochemistry of carbohydrates;* Wiley-Interscience: New York, 1971.
12. Ferro, D. R.; Provasoli, A.; Ragazzi, M.; Torri, G.; Casu, B.; Gatti, G.; Jacquinet, J. C.; Sinay, P.; Petitou, M.; Choay, J. *J. Am. Chem. Soc.* **1986**, *108*, 6773-6778.
13. Thatcher, G. R. J.; American Chemical Society. National meeting; American Chemical Society. Division of Carbohydrate Chemistry In *The anomeric effect and associated stereoelectronic effects;* ACS symposium series; American Chemical Society: Washington, 1993; Vol. 539.
14 .Dabrowski, J.; Kozar, T.; Grosskurth, H.; Nifant'ev, N. E. **1995**, *117*, 5539.
15. Wolfe, S. *Acc. Chem. Res.* **1972**, *5*, 102-111.
16. Lutteke, T.; Frank, M.; von der Lieth, C. W. *Nucleic Acids Res.* **2005**, *33*, D242-6.
17. Keeler, J. In *Understanding NMR spectroscopy;* John Wiley: Chichester, 2005.
18. York, W. S.; Hantus, S.; Albersheim, P.; Darvill, A. G. *Carbohydr. Res.* **1997**, *300*, 199-206.
19. Kupce, E.; Nishida, T.; Freeman, R. *Prog Nucl Magn Reson Spectrosc* **2003**, *42*, 95-122.
20. Kupce, E.; Nishida, T.; Widmalm, G.; Freeman, R. *Magn. Reson. Chem.* **2005**, *43*, 791-794.
21. Kupce, E.; Freeman, R. *J. Magn. Reson.* **2005**, *172*, 329-332.

22. Soderman, P.; Jansson, P. E.; Widmalm, G. *Journal of the Chemical Society-Perkin Transactions 2* **1998**, 639-648.
23. Jansson, P. E.; Stenutz, R.; Widmalm, G. *Carbohydr. Res.* **2006**, *341*, 1003-1010.
24. Karplus, M. *J. Chem. Phys.* **1959**, *30*, 15-18.
25. Cloran, F.; Carmichael, I.; Serianni, A. S. *J. Am. Chem. Soc.* **1999**, *121*, 9843-9851.
26 Haasnoot, C. A. G.; de Leeuw, F. A. A. M.; Altona, C. *Tetrahedron* **1980**, *36*, 2783-2792.
27. Wang, A. C.; Bax, A. **1995**, *117*, 1813.
28. Bose, B.; Zhao, S.; Stenutz, R.; Cloran, F.; Bondo, P. B.; Bondo, G.; Hertz, B.; Carmichael, I.; Serianni, A. S. *J. Am. Chem. Soc.* **1998**, *120*, 11158-11173.
29. Marquez, B. L.; Gerwick, W. H.; Williamson, R. T. *Magn. Reson. Chem.* **2001**, *39*, 499-530.
30. Meissner, A.; Sorensen, O. W. *Magn. Reson. Chem.* **2001**, *39*, 49-52.
31. Koźminski, W.; Nanz, D. *Journal of Magnetic Resonance,* **2000**, *142*, 294-299.
32. Koźminski, W.; Nanz, D. *Journal of Magnetic Resonance,* **1997**, *124*, 383-392.
33. Thrippleton, M. J.; Keeler, J. *Angew. Chem. Int. Ed Engl.* **2003**, *42*, 3938-3941.
34. Kupce, E.; Nishida, T.; Widmalm, G.; Freeman, R. *Magn. Reson. Chem.* **2005**, *43*, 791-794.
35. Kupce, E.; Nishida, T.; Freeman, R. *Progress in Nuclear Magnetic Resonance Spectroscopy,* **2003**, *42*, 95-122.
36. Nishida, T.; Widmalm, G.; Sandor, P. *Magn. Reson. Chem.* **1996**, *34*, 377-382.
37. Laatikainen, R.; Niemitz, M.; Weber, U.; Sundelin, J.; Hassinen, T.; Vepsalainen, J. *Journal of Magnetic Resonance Series a* **1996**, *120*, 1-10.
38. Claridge, T. D. W. In *High-resolution NMR techniques in organic chemistry;* Tetrahedron organic chemistry series; Elsevier: Amsterdam; London, 2009; Vol. 27.
39. Kowalewski, J., Mäler, L. **2006**, 2, 426.
40. Lipari, G.; Szabo, A. *J. Am. Chem. Soc.* **1982**, *104*, 4546-4559.
41. Mandel, A. M.; Akke, M.; Palmer, I.,Arthur G. *J. Mol. Biol.* **1995**, *246*, 144-163.
42. Hwang, T. L.; Shaka, A. J. *J. Magn. Reson.* **1998**, *135*, 280-287.
43. Kjellberg, A.; Widmalm, G. *Biopolymers* **1999**, *50*, 391-399.
44. Thomas, P. D.; Basus, V. J.; James, T. L. *Proc. Natl. Acad. Sci. U.S.A.* **1991**, *88*, 1237-1241.
45. Cohen, Y.; Avram, L.; Frish, L. *Angew. Chem. Int. Ed Engl.* **2005**, *44*, 520-554.
46. Stejskal, E. O.; Tanner, J. E. *J. Chem. Phys.* **1965**, *42*, 288-+.
47. Eklund, R.; Widmalm, G. *Carbohydr. Res.* **2003**, *338*, 393-398.
48. Guvench, O.; Hatcher, E.; Venable, R. M.; Pastor, R. W.; MacKerell, A. D., Jr. *Journal of Chemical Theory and Computation* **2009**, *5*, 2353-2370.
49. Hatcher, E.; Sawen, E.; Widmalm, G.; MacKerell, A. D.,Jr *J Phys Chem B* **2011**, *115*, 597-608.
50. Hinchliffe, A. In *Molecular modelling for beginners;* Wiley: Chichester, 2003.
51. Sattelle, B. M.; Hansen, S. U.; Gardiner, J.; Almond, A. *J. Am. Chem. Soc.* **2010**, *132*, 13132-13134.

52. Murphy, K. J.; McLay, N.; Pye, D. A. *J. Am. Chem. Soc.* **2008**, *130*, 12435-12444.
53. Ferro, D. R.; Provasoli, A.; Ragazzi, M.; Casu, B.; Torri, G.; Bossennec, V.; Perly, B.; Sinay, P.; Petitou, M.; Choay, J. *Carbohydr. Res.* **1990**, *195*, 157-167.
54. Herrera, A. J.; Beneitez, M. T.; Amorim, L.; Canada, F. J.; Jimenez-Barbero, J.; Sinay, P.; Bleriot, Y. *Carbohydr. Res.* **2007**, *342*, 1876-1887.
55. Das, S. K.; Mallet, J. M.; Esnault, J.; Driguez, P. A.; Duchaussoy, P.; Sizun, P.; Herault, J. P.; Herbert, J. M.; Petitou, M.; Sinay, P. *Chemistry* **2001**, *7*, 4821-4834.
56. McCasland, G. E.; Furuta, S.; Durham, L. J. *J. Org. Chem.* **1966**, *31*, 1516-1521.
57. Arjona, O.; Gomez, A. M.; Lopez, J. C.; Plumet, J. *Chem. Rev.* **2007**, *107*, 1919-2036.
58. Cumpstey, I.; Gehrke, S.; Erfan, S.; Cribiu, R. *Carbohydr. Res.* **2008**, *343*, 1675-1692.
59. Kupce, E.; Freeman, R. *Journal of Magnetic Resonance,* **2003**, *163*, 56-63.
60. Ottiger, M.; Delaglio, F.; Bax, A. *Journal of Magnetic Resonance,* **1998**, *131*, 373-378.
61. Wasylish.R; Schaefer, T. *Canadian Journal of Chemistry-Revue Canadienne De Chimie* **1973**, *51*, 961-973.
62. Ghazarian, H.; Idoni, B.; Oppenheimer, S. B. *Acta Histochem.* **2011**, *113*, 236-247.
63. Srivastava, O. P.; Hindsgaul, O.; Shoreibah, M.; Pierce, M. *Carbohydr. Res.* **1988**, *179*, 137-161.
64. Bock, K.; Duus, J. Ø.; Hindsgaul, O.; Lindh, I. *Carbohydr. Res.* **1992**, *228*, 1-20.
65. Stenutz, R.; Carmichael, I.; Widmalm, G.; Serianni, A. S. *J. Org. Chem.* **2002**, *67*, 949-958.
66. Thibaudeau, C.; Stenutz, R.; Hertz, B.; Klepach, T.; Zhao, S.; Wu, Q.; Carmichael, I.; Serianni, A. S. *J. Am. Chem. Soc.* **2004**, *126*, 15668-15685.
67. Lycknert, K.; Edblad, M.; Imberty, A.; Widmalm, G. *Biochemistry* **2004**, *43*, 9647-9654.
68. Bose, B.; Zhao, S.; Stenutz, R.; Cloran, F.; Bondo, P. B.; Bondo, G.; Hertz, B.; Carmichael, I.; Serianni, A. S. *J. Am. Chem. Soc.* **1998**, *120*, 11158-11173.
69. Cumming, D. A.; Carver, J. P. *Biochemistry* **1987**, *26*, 6676-6683.
70. Cumming, D. A.; Carver, J. P. *Biochemistry* **1987**, *26*, 6664-6676.
71. Cumming, D. A.; Shah, R. N.; Krepinsky, J. J.; Grey, A. A.; Carver, J. P. *Biochemistry* **1987**, *26*, 6655-6663.
72. Spronk, B. A.; Rivera-Sagredo, A.; Kamerling, J. P.; Vliegenthart, J. F. G. *Carbohydrate Research,* **1995**, *273*, 11-26.
73. Sanders, D. A.; Moothoo, D. N.; Raftery, J.; Howard, A. J.; Helliwell, J. R.; Naismith, J. H. *J. Mol. Biol.* **2001**, *310*, 875-884.
74. Calarese, D. A.; Scanlan, C. N.; Zwick, M. B.; Deechongkit, S.; Mimura, Y.; Kunert, R.; Zhu, P.; Wormald, M. R.; Stanfield, R. L.; Roux, K. H.; Kelly, J. W.; Rudd, P. M.; Dwek, R. A.; Katinger, H.; Burton, D. R.; Wilson, I. A. *Science* **2003**, *300*, 2065-2071.

75. Olsson, U.; Sawen, E.; Stenutz, R.; Widmalm, G. *Chemistry-a European Journal* **2009**, *15*, 8886-8894.
76. Lütteke, T.; Frank, M.; von der Lieth, C. *Carbohydr. Res.* **2004**, *339*, 1015-1020.
77. Klepach, T. E., Thibaudeau, C., Carmichael, I., Serianni, A. S. *Biohemistry* **2002**, 41, 8970.
78. Lycknert, K.; Helander, A.; Oscarson, S.; Kenne, L.; Widmalm, G. *Carbohydr. Res.* **2004**, *339*, 1331-1338.
79. Peters, T. *Liebigs Ann. Chem.* **1991**, *1991*, 135-141.
80. Stevens, E. S. *Biopolymers* **1994**, *34*, 1403-1407.
81. Case, D. A.; Scheurer, C.; Bruschweiler, R. *J. Am. Chem. Soc.* **2000**, *122*, 10390-10397.
82. Haasnoot, C. A. G.; de Leeuw, F. A. A. M.; Altona, C. *Tetrahedron,* **1980**, *36*, 2783-2792.
83. Donders, L. A.; De Leeuw, F. A. A. M.; Altona, C. *Magn. Reson. Chem.* **1989**, *27*, 556-563.
84. Altona, C.; Ippel, J. H.; Hoekzema, A. J. A. W.; Erkelens, C.; Groesbeek, M.; Donders, L. A. *Magn. Reson. Chem.* **1989**, *27*, 564-576.
85. Zhao, H.; Carmichael, I.; Serianni, A. S. *J. Org. Chem.* **2008**, *73*, 3255-3257.
86. Chou, J. J.; Case, D. A.; Bax, A. *J. Am. Chem. Soc.* **2003**, *125*, 8959-8966.
87. Tvaroska, I.; Hricovíni, M.; Petráková, E. *Carbohydr. Res.* **1989**, *189*, 359-362.
88. Delorme, C. *Int. J. Food Microbiol.* **2008**, *126*, 274-277.
89. Purwandari, U.; Shah, N. P.; Vasiljevic, T. *Int. Dairy J.* **2007**, *17*, 1344-1352.
90. Doco, T.; Wieruszeski, J. M.; Fournet, B.; Carcano, D.; Ramos, P.; Loones, A. *Carbohydr. Res.* **1990**, *198*, 313-321.
91. Lemoine, J.; Chirat, F.; Wieruszeski, J. M.; Strecker, G.; Favre, N.; Neeser, J. R. *Appl. Environ. Microbiol.* **1997**, *63*, 3512-3518.
92. Marshall, V. M.; Dunn, H.; Elvin, M.; McLay, N.; Gu, Y.; Laws, A. P. *Carbohydr. Res.* **2001**, *331*, 413-422.
93. Nordmark, E. L.; Yang, Z.; Huttunen, E.; Widmalm, G. *Biomacromolecules* **2005**, *6*, 105-108.
94. Kupce, E.; Freeman, R.; John, B. K. *J. Am. Chem. Soc.* **2006**, *128*, 9606-9607.
95. Ray, T. C.; Smith, A. R.; Wait, R.; Hignett, R. C. *Eur. J. Biochem.* **1987**, *170*, 357-361.
96. Beier, R. C.; Mundy, B. P.; Strobel, G. A. *Canadian Journal of Chemistry-Revue Canadienne De Chimie* **1980**, *58*, 2800-2804.
97. Damberg, P.; Jarvet, J.; Graslund, A. *J. Magn. Reson.* **2001**, *148*, 343-348.
98. Viel, S.; Capitani, D.; Mannina, L.; Segre, A. *Biomacromolecules* **2003**, *4*, 1843-1847.
99. Rolland, O.; Turrin, C.; Caminade, A.; Majoral, J. *New J. Chem.* **2009**, *33*, 1809-1824.
100. Mintzer, M. A.; Grinstaff, M. W. *Chem. Soc. Rev.* **2011**.
101. Tomalia, D. A. *Progress in Polymer Science* **2005**, *30*, 294-324.
102. Sousa-Herves, A.; Fernandez-Megia, E.; Riguera, R. *Chem. Commun. (Camb)* **2008**, *(27)*, 3136-3138.

103.Munoz, E. M.; Correa, J.; Fernandez-Megia, E.; Riguera, R. *J. Am. Chem. Soc.* **2009***, 131*, 17765-17767.

104.Sawa, M.; Hsu, T. L.; Itoh, T.; Sugiyama, M.; Hanson, S. R.; Vogt, P. K.; Wong, C. H. *Proc. Natl. Acad. Sci. U. S. A.* **2006***, 103*, 12371-12376.

105.Fernandez-Megia, E.; Correa, J.; Rodriguez-Meizoso, I.; Riguera, R. *Macromolecules* **2006***, 39*, 2113-2120.

106.Caminade, A. M.; Laurent, R.; Majoral, J. P. *Adv. Drug Deliv. Rev.* **2005***, 57*, 2130-2146.

107.Ballauff, M.; Likos, C. N. *Angew. Chem. Int. Ed Engl.* **2004***, 43*, 2998-3020.

108.Schaefer, J. *Macromolecules* **1973***, 6*, 882-888.

109.Meltzer, A. D.; Tirrell, D. A.; Jones, A. A.; Inglefield, P. T. *Macromolecules* **1992***, 25*, 4549-4552.

110.Meltzer, A. D.; Tirrell, D. A.; Jones, A. A.; Inglefield, P. T.; Hedstrand, D. M.; Tomalia, D. A. *Macromolecules* **1992***, 25*, 4541-4548.

111.Fernandez-Megia, E.; Correa, J.; Riguera, R. *Biomacromolecules* **2006***, 7*, 3104-3111.

112.Lipari, G.; Szabo, A. *J. Am. Chem. Soc.* **1982***, 104*, 4559-4570.

113.Wu, D. H.; Chen, A. D.; Johnson, C. S. *Journal of Magnetic Resonance, Series A* **1995***, 115*, 260-264.

114.Rietveld, I. B.; Bedeaux, D. *Macromolecules* **2000***, 33*, 7912-7917.

115.Markelov, D. A.; Lyulin, S. V.; Gotlib, Y. Y.; Lyulin, A. V.; Matveev, V. V.; Lahderanta, E.; Darinskii, A. A. *J. Chem. Phys.* **2009***, 130*, 044907.

116.Poveda, A.; Martin-Pastor, M.; Bernabe, M.; Leal, J. A.; Jimenez-Barbero, J. *Glycoconj. J.* **1998***, 15*, 309-321.

117.Malveau, C.; Baille, W. E.; Zhu, X. X.; Ford, W. T. *Journal of Polymer Science Part B-Polymer Physics* **2003***, 41*, 2969-2975.